JOINT EUROPEAN TORUS JET

JET–P(92)46

A. Kaye, T. Brown, V. Bhatnagar, P. Crawley, J. Jacquinot,
R. Lobel, H. Panissie, J. Plancoulaine, P-H. Rebut, T. Wade,
C. Walker and JET Team

Present and Future JET ICRF Antennae

Present and Future JET ICRF Antennae

A. Kaye, T. Brown, V. Bhatnagar, P. Crawley, J. Jacquinot, R. Lobel, H. Panissie, J. Plancoulaine, P-H. Rebut, T. Wade, C. Walker and JET Team*

JET-Joint Undertaking, Culham Science Centre, OX14 3DB, Abingdon, UK

** See Annex*

Preprint of Paper to be submitted for publication in
Fusion Engineering and Design

PRESENT AND FUTURE JET ICRF ANTENNAE

A Kaye, T Brown, V Bhatnagar, P Crawley, J Jacquinot, R Lobel, H Panissié, J Plancoulaine, P-H Rebut, T Wade, C Walker

JET Joint Undertaking, Abingdon, Oxon OX14 3EA

Since the initial operation of the JET ICRF system in 1985, up to 22 MW has been coupled to the plasma, many heating scenarios have been demonstrated and the main technological problem of RF-specific impurity production overcome. Many developments of the antennae have taken place over this period, notably the replacement of the water-cooled nickel screens with indirectly cooled beryllium screens, and the forthcoming installation of eight new A2 antennae for operation during the pumped divertor phase of JET. The A2 antennae include enhanced provision for fast wave current drive experiments on JET. This paper describes the beryllium screens, the technological results from operation and subsequent inspection of these screens, the design of the A2 antennae and the results from high power RF testing of a model of the A2 antenna.

1 Introduction

A system for ion cyclotron heating has been operational on JET since 1985. The initial prototype system comprised two uncooled antennae and two generators each producing 3 MW of power at the generators [1]. Subsequent developments have seen the number of antennae and generators increased to eight, the prototype antennae replaced by the eight water-cooled, so-called A1 antennae with nickel screens [2], in turn replaced by beryllium screens [3], and the generators upgraded to 4 MW each [4]. Thus, the system as operational until February 1992 comprised eight beryllium screened antennae and a total of 32 MW of power at the generators.

This ICRF system has achieved a wide range of results on JET, including the coupling to the plasma of power in excess of 22 MW for 2 seconds, the coupling of 200 MJ in a single pulse, operation for 60 s [5], the reduction of all impurities from the antennae to negligible levels and the development of a model of impurity production which is consistent with the observations [6-8], production of RF only H-modes [9,10], development of the pellet-enhanced H-mode [11], operation at 90 degree phase shift between conductors and the related first observation of evidence for fast wave ion current drive [12]. Many varying modes of operation have been explored [13], including the discovery of synergistic effects with lower hybrid current drive [14].

The last campaign of operation on JET finished in February 1992 for installation of the pumped divertor [15]. This new configuration of JET produces a plasma profile which is substantially further from the wall than at present. In order to achieve adequate coupling to this new plasma, a new set of antennae, the so-called A2 antennae [16,17], is being manufactured and will be installed in JET along with the pumped divertor. These antennae incorporate a number of novel features arising from the requirements to minimise the disruption forces on the antennae, to increase the coupling and to enhance fast wave current drive experiments on JET. The control, protection and, in particular, the matching of the generators is also being upgraded.

This paper describes the A1 antennae with beryllium screens which operated in JET up to February 1992, and also the new A2 antennae which will be operating in JET after the present shutdown. The upgrading of the generators and their control, protection and matching systems is described elsewhere in this edition.

2 The Requirements of the JET Antennae

The decision to have a substantial ICRF system on JET was taken after the basic machine had been designed and manufactured. The specification for this RF system is given in table 1 as originally conceived and as presently defined.

A total of 15 MW was to be coupled to the plasma using ten antennae, each being driven by two 1.5 MW tetrodes. The number of antennae was reduced to eight after initial encouraging results on the prototype system, and the tetrode power was upgraded to 2 MW when such tubes became available. The location of the antenna around the torus is shown in Fig 1a.

The RF system had to be compatible with the existing torus design, in particular to utilise the available ports for access to the torus and to be accommodated within the 150 mm gap between the plasma boundary and the torus wall. Designs utilising transmission line access through either the main horizontal ports or the so-called limiter guide tubes were considered. The latter tubes are c. 150 mm diameter x 2 m long, located in pairs on either side of the main ports, and provide radial access to the torus. It was concluded that the full output power from one tetrode could be coupled through one of these tubes at typical standing wave ratios, and the decision was therefore taken to use these tubes for access, avoiding the option of using a 'plug' type of construction, with the antennae being projected as an assembly into the torus Rather the antennae had to be inserted into the torus through a main port and assembled onto the wall from inside. This freed the main ports and enabled the size of the antennae to be increased to a limit set by access through the port at the most convenient orientation, and led to the evolution at JET of a series of large, low power density designs.

The ICRF system was required to be used during the planned tritium phase. This required the co-axial line and the windows in particular to be immune to the anticipated neutron

flux, and also required that the antennae be replaceable remotely, using the JET robotic facilities, should this turn out to be necessary.

The requirement to fit into the existing gap between the plasma and the torus limited the coupling resistance that could be achieved and thus the maximum spacing that could be allowed between the antenna and the plasma boundary whilst maintaining adequate coupling. The system was conceived to have a maximum zero-to-peak RF voltage capability on the transmission lines and antennae of 50 kV. This would enable the maximum power to be coupled at a coupling resistance of 1.1 ohms or above, where the coupling resistance is defined to be the resistance which, when placed at a current maximum in the line, is equivalent to the resistive component of the antenna impedance.

The poloidal profile of the antennae was chosen to be parallel to, and about 20 mm outside of, the magnetic surface tangential to the toroidal limiters with a plasma elongation of 1.6. This surface is essentially parallel to the torus wall.

3 The A1 Antennae

3.1 Background Information

The so-called A1 antennae were designed to meet the full JET specification in Table 1 above. These antennae were installed in JET in 1987 with nickel screens. These screens were cooled by water flowing through channels in each screen element and have been previously described [1]. These screens were replaced by beryllium screens in 1990, with the objectives of reducing the ion impurities released to the plasma during RF operation and improving the integrity of the system against water leaks. This paper describes only the beryllium screen version of the A1 antennae.

3.2 *General Description*

A vertical section through the A1 antenna is shown in Fig 2. Two co-axial vacuum transmission lines (VTL) connect the incoming pressurised 225 mm diameter co-axial lines via double vacuum windows, through the access tube to the torus wall, where they connect to the back of the antenna housing. Each line connects to one of the two central conductors of the antenna, and is supported at the torus end by a conical ceramic. The antenna housing is mounted on the torus wall and contains two central conductors, one for each VTL. The housing also carries the screen which is mounted between the central conductors and the plasma, as seen in the horizontal section of the antenna shown in Fig 3. The screen in turn carries graphite tiles on each side to protect the screen elements from the plasma.

During installation of the antenna, the housing is inserted into the torus on the Remote Handling boom through one of the main ports and positioned onto the torus wall. The two VTL's are then inserted into the tubes from outside of the torus and connected to the antenna by a 60 degree rotation using bayonet connectors. The screen is subsequently entered into the torus, also using the boom, and mounted on the front face of the housing. The water connections to the toroidal limiters are welded using automatic tools. The protection tiles are installed last.

An active metal getter pump [18] of c. 500 l/second pumping speed is provided on each VTL due to the low conductance of the VTL to the torus past the conical ceramic. This getter pump maintains the VTL pressure below 10^{-5} mbar during normal operation of the system. It is regenerated into the torus by baking to 500 C.

3.3 *RF Design of the Antennae*

The incoming transmission line has a diameter of 225 mm and a characteristic impedance of 30 ohms. It attaches to the vacuum window. This window utilises two conical ceramics and generous corona rings to minimise the field enhancement by the high dielectric alumina ceramic, and has a reduced inner conductor diameter to match the impedance. All windows used on JET have been individually tested at maximum voltage, and type tested at maximum current for 20 seconds.

A complete VTL is also shown in Fig 2. It incorporate a bellows on the inner conductor for thermal expansion. This has rather flat convolutions to reduce field enhancements, and has been designed to match the line impedance These bellows have been type tested at maximum current and voltage.

The torus end of the VTL is supported by a conical ceramic which is held in compression by a spring disc stack at the outer end of the VTL, reacted onto the access tube flange. The ceramic is supported on helicoflex seals with silver sheaths. These seals provide a compliant land and also a good RF contact to the ceramics. The ceramics are also metallised with silver where they contact the seals in order to avoid field concentrations in this region. The line diameter is reduced at the conical ceramic, following the refraction of the equipotentials in the cone whilst maintaining the line impedance The inner diameter of the outer conductor as it enters the access tubes is 120 mm, reducing to 90 mm at the conical ceramic, this being at a region of high voltage on the line.

The VTL connects to the housing and the central conductor again using silver helicoflex seals in compression to establish good RF contact. The connection to the central conductor is compressed using a screwed shaft inside the VTL, whilst the housing connection uses the same seal as the conical ceramic and is compressed by

the axial load on the ceramic. These seals operate at high temperature in high vacuum and tend to diffusion bond during operation. Dismantling of the lines almost invariably destroys the seals and leaves debris on the faces. A thin coating of palladium has been applied to alleviate this problem and is partly effective. Carbonisation of the seal face is being explored as an alternative.

The central conductors are of a convoluted shape as shown in Fig 4. Each conductor splits into two current straps operating in parallel and displaced poloidally from each other in order to obtain a more uniform current distribution. This arrangement allows operation of the antenna as a toroidal dipole (peak $k_{||} = 7/m$) or monopole ($k_{||} = 0$), whilst remaining a monopole in the poloidal direction. The corresponding $k_{||}$ spectra are shown in Fig 12a. This gives improved coupling relative to the so-called quadruple conductor configuration used previously [1]. The dimensions of the central conductor straps have been chosen to optimise the current split over the required range of frequency, and to approximately match the line impedance. This design has been checked using a full scale flat model of the antenna, including the screen. Typical measured current distributions are given in [1]. As with the VTL, the mechanical attachments to the housing at the short circuits utilise helicoflex seals to establish good RF contact. The conductors are made from typically 20 mm thick inconel plate. All surfaces of the conductors are rounded to a minimum radius of 10 mm, and clearance to the housing measured along the magnetic field is kept above 25 mm. This is marginally adequate as some arcing has been observed along the field lines in the antennae. The clearance normal to the magnetic field is kept above 12 mm minimum and this appears to be quite sufficient. All surfaces are electro-plated with 100 microns of silver to reduce RF losses.

The screen is positioned to leave a gap of 12 mm to the central conductor. It comprises an open structure of c. 23 x 23 mm beryllium rods as described in detail below. The screen assembly is connected to the housing by a series of spring contacts. These

comprise nimonic springs as shown in Fig 5, coated in 5 microns of silver (about half of the skin depth). These contacts serve to establish RF contact between the screen and housing, allowing capacitively and inductively driven RF currents to flow at a level of typically a few x 10 amps per spring without overheating. The resistance is however sufficient at low frequencies to substantially reduce the eddy currents flowing during a plasma disruption and thus reduce the forces on the screen elements. These contacts have been found to perform very satisfactorily in practice. No damage to the contacts or the screen elements has been observed.

3.4 *Mechanical Design*

The A1 antenna is designed to be installed and removed using remote handling tools. The attachments between component parts and to the torus have therefore been simplified as far as possible. The antenna is located relative to the torus using conical spigots in the VTL access ports. An outward radial load of 70 kN is applied by the VTL to each spigot, which pulls down onto helicoflex seals as shown in Fig 6. At the upper spigot, the seals occupy only the lateral quadrants, allowing a small differential expansion in spigot pitch relative to the torus. These spigots fully define the position of the antenna and no adjustment is made in the torus to accommodate tolerances. Survey after installation shows a variation of 3 mm in radial position of the centre of the screen and up to 6 mm at top and bottom due to amplification of small vertical alignment errors in the spigots.

The in-torus components are subject to substantial forces during disruptions due to induced eddy currents. The main component [19] is a torque about a radial axis arising from the eddy current circulating along the screen elements and closing around the back of the housing. The spigots can support this load. However, there is also a substantial twist induced in the housing about a vertical axis. Being an open box, the housing is not stiff to such a twist and additional support from the torus is

required. In addition, vertical disruptions induce a torque about a vertical axis, which again cannot be supported by the spigots. Additional attachments to the torus are therefore provided at each corner of the housing. These support the housing radially to within 3 mm. This clearance is left to accommodate distortion of the torus itself. These supports allow sliding movement in the vertical plane to accommodate differential expansion. A bayonet design is used to facilitate remote installation.

In addition to the global forces, the forces arising on the individual screen elements are important. Typically, the elements are designed to accommodate radial loads of 1200 N per element and a torque about a radial axis of 500 Nm, equivalent to a lateral force of 800 N at each end of the element. Sample beryllium elements have been tested to destruction at both room temperature and 400 C. These failed at the equivalent loads of 3000 N and 1660 N respectively, the former due to brittle fracture and the latter by fully plastic yield.

Forces on the central conductors are modest and readily accommodated given the use of typically 20 mm thick inconel plate to reduce the edge curvature. Thermal stress in the central conductor is avoided by use of a flexure pivot attachment at the outer short circuit. This comprises 1 mm inconel sheet typically 100 mm square. The attachment of this to the conductor must avoid RF current concentrations which can lead to failure of this section.

Disruption forces on the VTL are small. A bellows is included on the inner conductor to avoid thermal stress on the window. A second bellows is incorporated in the attachment to the tube flange to allow loading of the spigots using external disc springs, and also to accommodate thermal expansion. The conical support has been tested without failure up to an axial load of 70 kN.

3.5 *Thermal design*

All RF current carrying surfaces (except the screen elements) are electroplated with 50 - 100 microns of silver in order to reduce the RF losses to a minimum. On the VTL, the temperature rise during a single pulse is significant only on the inner bellows, and here is typically 100 C per 20-sec pulse at 50 kV. The inside of this bellows is air at 3 bar, and cooling occurs by convection between pulses. The steady state temperature of the VTL inner conductor would be excessive (greater than 500 C) with full duty cycle operation at a voltage above 40 kV. A closed loop gas cooling system can circulate 3 bar air from the basement to the antenna up one of the main co-axial lines, through the two VTL's on that antenna in parallel, and back to the basement in the other co-axial line. The main lines act as heat exchangers for the mean power of typically 200 watts per line. This loop has never been required in practice.

The central conductors were originally cooled by radiation to the water cooled screens. With the beryllium screens, the mean temperature of the elements may reach 300 C, which reduces the effectiveness of this cooling. Nonetheless, cooling of the central conductor by radiation is not a problem.

The Al nickel screens did not allow line of sight through the screens (Fig 7a). Experience at ASDEX [20] and JFT-2 had shown successful operation of screens with a clear line of sight. Allowing such a line of sight can much reduce the RF losses in the screen elements by allowing an increased gap between elements. Taking account both the effect of the improved conductivity of beryllium over nickel, and the effect of increasing the gap from 3 to 8 mm, with the element section shown in Fig 7b, the losses in the elements are reduced by an order of magnitude. This reduction in loss has been confirmed using calorimetric measurements on the prototype beryllium screen, which has a measured loss of 0.01 ohm. Adopting such an open design thus

renders possible the use of end-cooled beryllium elements on JET, which makes the beryllium screen feasible using existing technology.

A section through the beryllium screen is shown in Fig 8 and a photograph of the screen is shown in Fig 9. The elements are cooled partly by radiation and partly by conduction to the water-cooled end manifolds carrying the side protection. The attachments to the screen had to establish good thermal contact and yet allow typically 3 mm expansion of the element and support radial and lateral loads of 600 and 800 N respectively. A flexure pivot utilising copper-chrome-zirconium alloy was fabricated by electron beam welding foils into solid end fittings. The heat treatment had to be carefully controlled at all stages. The foils were rolled in solution heat treated condition, formed to the correct shape (different for each foil in a stack), welded to the end fitting also in solution heat treated condition, and finally age hardened at 450 C. These units were then assembled to the elements using heat shrunk nimonic rings with close control on the fit-up. All assemblies were load tested before use. In addition, sample assemblies were fatigue tested with change in length to 100,000 cycles, and load tested with 700 Nm torque about a radial axis. The assemblies were finally bolted to the screens using silver foil gaskets.

The screen is protected from the plasma by graphite tiles mounted on the side manifolds, and by the toroidal limiters top and bottom. The screen elements are 20 mm behind the magnetic surface tangential to the side protection, which is in turn 17 mm behind the limiter tiles for the design plasma elongation of 1.6. The elements are curved to follow the local magnetic surfaces, taking account of the toroidal field ripple. Direct plasma losses on the screen elements are then negligible. Inspection after plasma operation has shown no evidence of damage to the elements. Rather, a nett deposition of material onto most of the screen is observed.

3.6 *Testing before installation*

The following testing was carried out on components and complete antennae using the nickel screens:

- All vacuum RF windows were tested with 50 kV, 20-sec duration pulses with open circuit termination close to the window. The prototype was also type tested with closed circuit termination

- The prototype silver-plated VTL was type tested with 50 kV, 20-second pulses with both open and short circuit termination at the conical ceramic.

- A copper plated VTL was also tested at 50 kV. It was found that conditioning of this line was much more difficult than the silver-plated line. Conditioning was carried out by application of 10 millisecond, medium voltage pulses, with the voltage being reduced in steps until multipactor arcing occurred. The voltage was then held constant until no further multipactor arcing was observed, before again being reduced in steps. This process successfully conditioned the copper line, but only after many more pulses. Furthermore, after exposure to hydrogen at 10^{-3} millibar, it was necessary to recondition the line. No further work was therefore done with copper lines

- The prototype antenna was tested with 50 kV, 20-second duration pulses every ten minutes for two working days. A single generator was used with a T-junction to drive both VTL simultaneously, located such as to give monopole operation. This test showed consistent and reliable operation at this voltage. Subsequently, after observation of voltage limits in the torus, tests showed no clear degradation in maximum voltage with increasing pressure of hydrogen up to the onset of glow discharges in the test vessel at pressures approaching 10^{-3} mbar.

RF testing of the beryllium screens before installation was limited by the available time to demonstration of no arcing up to 35 kV (limited by the pressurised transmission lines), and calorimetric confirmation of the low losses in the screens (typically 0.01 ohms).

4 Operating Experience

No attempt is made here to present the physics results obtained with these antennae. Rather, the limits to the power handling capability observed on the torus and the observations of metal impurities arising from the antenna will be reviewed

4.1 *Limitations on Coupled Power*

Notwithstanding the good performance observed in the test bed, it has been found in practice that reliable operation is obtained only up to a maximum of about 30 kV.

The limitation on peak voltage on the antenna itself appears to be the conical ceramic, cf Fig 6 above. This ceramic is located close to a voltage maximum and in a region of reduced line diameter. Arcing is observed parallel to the magnetic field at the corona rings adjacent to the ceramic and in the reduced diameter line towards the antenna. This leads to deposition of metal onto the ceramic and ultimately to persistent arcing at, and excessive reflection from, the ceramic. The corona rings have been modified on all antenna to reduce the local field concentration with little improvement. The maximum electric field which has been reliably sustained in the torus environment parallel to the magnetic field is about 2.2 kV/mm. Attempts to simulate this arcing in the test bed (without magnetic field) have been unsuccessful.

Occasional arcing has also been observed between the central conductors and the adjacent short circuit connection at the centre of the antenna, again parallel to the magnetic field. The electric field parallel to the magnetic field is typically 1.6 kV/mm in this region at maximum operating voltage

A clear limit that has been identified on the JET system is with VTL pressure. Arcing with occasional catastrophic consequences has been consistently observed if this pressure exceeds a few times 10^{-4} mbar. A hard interlock is provided on this pressure which removes RF power. The response time of the detectors and of the pressure to events in the VTL is relatively slow (0.1 second) and severe damage can occur in this time.

The system voltage limit depends on the frequency, apparently in a manner which correlates with voltage at particular locations in the generators [22] subsequent to arcing in the antenna or transmission line. The limit also appears to depend on the level of crosstalk between antennae, which is in turn dependent on the level of damping in the plasma.

It is clear that a full understanding of the limits must take account of the complete antenna array, and of the detailed interaction between the antennae and the generators. Results obtained on the test bed cannot be achieved on the torus, and the latter have not been reproducible on the test-bed. A conservative approach must therefore be taken in both designing and testing new antennae. The JET results suggest a downgrading by a factor two in voltage of the test bed results for reliable torus operation.

One area requiring close attention in the design stage is arc protection when using automatic matching systems. These systems greatly facilitate torus operations and are essential for next generation systems, but the system must prevent matching to

arcs which can have severe consequences. Optical interlocks may be a solution, but is difficult to implement. The chosen system for the next campaign on JET is to limit the amplitude of frequency tracking to ±200 kHz. This will accommodate the plasma load variations but will not allow matching to an arc near the ceramic, which requires 900 kHz.

4.2 *Coupling Resistance*

JET define the coupling resistance to be the equivalent resistance located at a current maximum in the 30 ohm transmission line. The predicted and measured coupling resistance have previously been shown to agree satisfactorily [19]. For a given mode of operation (monopole or dipole), the coupling resistance is largely determined by the edge density and density gradient, which in turn strongly depend on the distance from the screen to the plasma. The limits to voltage found on JET imply limits on the coupling resistance. The JET system has coupled 22 MW, but can only achieve this if the plasma is close to the antenna to give a coupling resistance greater than 5 ohms. This has not been achieved with some operating scenarios on JET, notably low density single null configurations. Nonetheless, up to 12 MW of power has been coupled to these plasmas.

4.3 *Impurity Release during RF Heating*

Early ICRF systems suffered consistently from the appearance of impurities in the plasma during RF operation. Based partly on observations at JET, including using a Langmuir probe in one of the earlier nickel screen elements, a model for the mechanism involved has been developed [6-8].

This model is consistent with observations on a number of experiments. The impurities arise from sputtering, including self-sputtering, at the rectified sheath on

the screen elements and protection tiles. These arise when nett RF flux crosses closed loops formed by tilted field lines intersecting the screens and tiles. The metallic impurities can be avoided by using materials of low self sputtering yield in the 0.1-1 kV range (such as beryllium), or by avoiding the appearance of nett RF fluxes, for example by operating in dipole configuration or tilting the screen elements. The increase in Z_{eff} in JET specific to the ICRF with the tilted beryllium screens has been shown to be of the order 0.005 per MW in monopole, and 0.001 per MW in dipole. This is negligible.

4.4 *Inspection after Operation*

The A1 antennae have now been removed from JET. Observations before and during removal were as follows:

- The antenna screen elements, and attachments were all in excellent condition, with no significant damage. The elements were largely coated in a layer of evaporated beryllium, with an orange-brown surface layer thought to be beryllium carbide. Only local minor erosion of the elements was observed.

- Stripes of evaporated beryllium were clearly visible on the central conductor and inside of the housing, corresponding to the gaps between screen elements. There was no evidence of arcing associated with these stripes.

- The spring contacts were all in as-new condition.

- Some arcing was observed from the central conductors to the housing and to the central short circuits, as previously noted.

- Some tenuous but repetitive arc damage was observed between the screen and housing, the screen and the belt limiters, and the housing and the torus wall.

- Severe damage was observed at the conical ceramics on two lines, due to failure of the arc protection circuit as previously noted.

These observations confirm the remarks in Section 4.1 above regarding the limitations on performance. The clear evidence for net deposition of material onto the bulk of the beryllium screen may not be consistent with the conventional modelling of erosion effects of disruptions with components on the outer wall.

5 Design of the A2 Antenna

5.1 *Background Information*

With the installation of the pumped divertor in JET [15], the plasma volume is substantially reduced and, in particular the distance from the plasma to the wall is increased by about 300 mm or 450 mm for the 'fat' and 'thin' plasma configurations respectively. With this clearance, the coupling of the A1 antennae is too low to be useful. Furthermore the curvature of the plasma is changed and it is no longer symmetrical about the centreline, as shown in Fig 10. A new set of eight A2 antennae is therefore being manufactured for use in this configuration [16,17]. These antennae are as large as can be installed through the port, being a factor 1.5 larger in width and a factor 2 in depth compared to the A1 antennae. The toroidal positions of the antennae in the torus are being re-arranged to give two diagonally opposite groups each of four adjacent antennae to improve the directivity of the launched wave. The opportunity has also been taken to remove the conical ceramic which limits the voltage of the A1 antennae, and the design is such as to enhance the coupling

capability, and also the directivity of the spectrum for fast wave current drive experiments.

The duty cycle required of these antennae has been reduced to 1:60, reflecting limits elsewhere in JET, although the 20-second pulse duration is retained. The remote handling requirement has also been reduced to a minimum. Only capping of the windows in order to maintain torus integrity in the event of a window failure is required to be done remotely. The peak RF design voltage for thermal analysis is reduced to 42 kV, reflecting previous experience and the improved coupling of the A2 antenna. A summary specification of the A2 antennae is given in table 2.

5.2 *RF Design*

The radial depth and the toroidal extent of the antenna have been maximised to improve the coupling resistance. A section through one antenna is shown in Fig 11. The height is effectively determined by the frequency and is similar to the A1 antenna. In order to optimise the spectrum near the centreline, the antenna is shaped as part of a sector of the torus, not as a rectangular box. The width of the antenna therefore reduces with major radius towards the bottom of the antenna. The tilt of the magnetic field changes from 13 degrees to 18 degrees with height, and the screen elements are set at varying angles to follow this field. Each antenna has two central conductors as shown in Fig 12. These are similar to the A1 conductors, each with two loops connected in parallel to give a poloidal monopole. Unlike the A1, the two loops are both terminated at the top, giving toroidal monopole operation with zero phase difference. A septum is introduced between the two conductors in order to reduce the coupling between adjacent conductors and facilitate matching at arbitrary phase between conductors. The sidewalls and the septum are slotted to a depth of 104 mm and 100 mm respectively from the screen front face in order to minimise degradation

of the spectrum by the image currents in these components. The adjacent tiles on the poloidal limiter are similarly slotted.

A full scale flat model of the new antenna has been used to check the distribution of RF current in the central conductors. Typical results are shown in Fig 13 after optimisation of the conductor shape. The two conductors are not identical in their connection to the VTL as the antenna centreline is displaced toroidally from the incoming lines. This has required a relative displacement in the poloidal position of the central crossover. Some asymmetry in current appears between top and bottom at the highest frequency.

Typical spectra calculated to be produced by this antenna [22,23] are shown in Fig 14, together with the corresponding directivity. Typical values for A1 are also shown in Fig 14. The improvement with A2 is up to a factor 1.3 (at a phase shift c 70 degrees between straps). The directivity of the A2 antenna is anticipated also to be much more tolerant of adverse plasma conditions, such as low damping per pass, which will degrade the A1 directivity.

The computed coupling resistance for A2 is shown in Fig 15. These results are typically a factor 1.5 to 2 higher than A1 for the same separation between the screen and plasma, due to the increased width and depth of the antenna.

The conical ceramic supporting the inner conductor of the VTL has been deleted in the new design, a cylindrical ceramic inside the antenna housing being substituted, see Fig 13 above. This leaves the VTL clear of all ceramics apart from the window, which is remote from the voltage maximum except at the extremes of frequency. The new ceramic remains close to the voltage maximum, but the electric field is reduced with this design and at no point on the surface is the electric field parallel to the magnetic field. This configuration has been successfully tested to 50 kV with 20-second pulses.

The ceramic is alumina with metallised ends, resting on helicoflex seals. As the VTL is now open to the torus, no additional pumping is provided. The time constant for evacuation of the VTL to the torus is less than 1 second. The previous getter pumps are retained for pumping the interspace on the double windows, which are being re-used. With the reduction in duty cycle and voltage, the VTL gas cooling system is no longer required.

5.3 *Thermal Design*

The successful operation of the beryllium screens has confirmed the acceptability of open screen structures on JET. The A2 antennae retain this feature, with a single row of straight 24 mm diameter round beryllium bars spaced with a 5 mm gap (see Fig 7c). The RF losses in these elements are similar to the A1 beryllium screen, equivalent to 0.01 ohms coupling resistance. Consequently, cooling of the screens can be achieved using only radiation to the torus. The losses in the central conductors and the housing similarly can be accommodated using only radiation. There is therefore no active cooling of these antennae. This leads to considerable simplification of the design, and is the justification for downgrading the remote handling requirements.

As described below, the housing is fabricated from thin (0.8 - 3 mm) sheet metal. Consequently, the temperature of the housing may reach 600 C, with hot spots up to 700 C, when the torus is at 350 C. At this temperature, the vapour pressure and diffusion of silver are starting to become a problem. Further, the required thickness of silver would significantly reduce the resistance of the housing to disruption induced eddy currents, with consequent increase in the forces. The RF surfaces of the housing and central conductors are therefore coated with nickel rather than silver as previously, the increased losses being more than compensated by the higher emissivity in a radiation cooled system. A nickel coated test assembly has been

successfully tested up to 50 kV. Conditioning has been similar to silver coated antennae, typically 3 hours of pulsing to achieve full performance.

5.4 *Mechanical Design*

The A2 antennae are required to couple to the pumped divertor plasma. As this plasma is far from the torus wall, the antennae are required to similarly project far into the torus where they are exposed to the full rigours of disruption-induced eddy currents and the resulting forces. Further, the new plasma configuration is anticipated to have a faster current decay. An antenna of similar construction to the A1 is estimated to develop forces of order 500 kN at each corner, forces which would have to be supported by the torus wall. The antenna mechanical design has therefore been driven by the need to reduce the stresses in the wall to acceptable levels. This has been achieved by:

- using thin sheet material to fabricate the housing, with a flexible design to accommodate consequent thermal and disruption induced bending.

- incorporating resistors in series with the screen elements in order to reduce eddy currents flowing in the screen to acceptable level.

- using distributed articulated attachments to the torus to support the antenna whilst allowing differential thermal expansion.

- using a lightweight but rigid central conductor to minimise disruption forces, avoid collision with the screen and help support the housing and the VTL.

The resulting antenna is illustrated in figures 11 above and 16. The housing has a rigid tubular septum which carries the screen supports and central conductor

attachments. The two halves of the housing have a convoluted construction which allows flexing to accommodate differential expansion, and also to follow flexing of the torus wall. These convolutions are attached to the torus by many electrically isolated, pin-jointed arms, which support the antenna against radial and toroidal loads whilst allowing thermal expansion. Vertical loads are supported by a separate linkage adjacent to the VTL attachments.

The sides of the antenna are protected by the new poloidal limiters being installed in JET. The last closed flux surface on the face of these tiles is 20 mm and 21 mm respectively in front of the centre of the beryllium elements on the two halves of the antenna, as shown in Fig 17.

The central conductor has a rigid, hollow section construction of large moment of inertia. This is necessary to support the conductor and the housing against disruption forces. The ceramic attaching the conductor to the housing also supports the radial load on the VTL arising from the 3 bar line pressure acting on the inner bellows. The inside of the conductor is vented to the torus outside the antenna housing. The four conductors in each pair of antennae are mounted at nearly constant toroidal pitch, as also shown in Fig 17.

The screen elements are mounted in pairs, each attached to the housing via a ceramic resistor. This resistor, which is necessary in order to reduce disruption induced currents, comprises an alumina ceramic block with a thin coating of nickel (about 5 microns). The resistance at 300 C is 0.15 ohms, with a tolerance of +/- 5 %. Sample resistors have been tested extensively both with applied RF power and using a capacitor bank to simulate eddy currents. The performance required and measured during tests is shown in Table 3.

The performance is seen to meet the requirements but with a rather narrow margin in RF current. The initial failure mode is arcing which originates at current concentrations at the edge of the metal coating and which leads to highly local evaporation of the metal. This enhances the local current concentration and leads to propagation of a break in the metallising across the resistor. Careful design to avoid current concentrations has improved the performance to that given in Table 3, where thermal stress cracking and the thermal diffusivity of the ceramic also limit performance. Further developments are proceeding. In particular, the use of beryllia ceramic appears to give a 30 - 40 % increase in the current limit.

The forces on the A2 antenna arising from disruptions are summarised in Fig 18. It is observed that the main force arises from a torque about a vertical axis, and amounts to typically 50 kN on each side of the antennae, or 5 kN per articulated support arm.

5.5 *RF Testing*

A full scale model of the upper VTL-side quadrant of the A2 antenna has been extensively tested on the JET RF test bed. This model incorporates many features of the full antenna, including the cylindrical ceramic, the resistors, nickel plating, and construction typical of the real antenna.

The beryllium screen elements of the A2 antenna are replaced by solid nickel elements. An additional feature of this 'Short Assembly' is the ability to be configured with the strap terminating in an open circuit (of smooth profile to prevent arcing). The strap in this case is only supported by the cylindrical support ceramic and the strap-to-screen gap is increased from 12 to 18 mm to eliminate arcing in the absence of a magnetic field.

The impedance of the Short Assembly was measured in short-circuit configuration and compared with that of a low power aluminium model of the full A2 antenna. The measured half and quarter wavelength resonances of both models are within a few MHz (see Table 4).

The test environment and equipment are detailed in Table 5, whilst the results achieved to date in the on-going test programme are summarised in Table 6.

The test programme has confirmed the viability of important aspects of the A2 design:

- There is no requirement for independent pumping of the VTL (except for the interspace of the double ceramic window): the pumping from the torus, estimated to be 100 l/second at the window, is sufficient to handle the out-gassing during RF pulses. Some form of bakeout and continuous heating along the VTL is however desirable. An interlock is necessary to prevent operation too early in the ramp up phase following the initial gas fill of the torus.

- The light weight, fabricated structure of the antenna still offers sufficient thermal heat capacity in the critical areas to limit temperature excursions to acceptable levels during RF pulses.

- With radiative cooling alone full power operation at up to 20:1 duty cycle is possible whilst operating in an ambient environment of 200 C (with no plasma load). The limit is excessive heating of the VTL Inner Conductor and the strap. The maximum JET duty cycle is 60:1.

current in the A2 screen elements will, on this basis, be similar to that in the

- Vertical displacement of screen elements up to +/-5 mm in operation due to distortion of the antenna housing or screen mounting posts has no impact on the antenna performance; however the currents in the ceramic screen resistors is increased and this must be allowed for in their design.

The RF test programme confirms that the RF currents flowing in the screen elements are both capacitive and inductive when tilted screen elements are employed. The expected current per element in the A2 design from the capacitive coupling between the closely spaced strap and screen elements can be calculated to be a maximum of 18 Amps rms flowing to the housing at each side of each element at 55 MHz with a peak line voltage of 42 kV. This corresponds to 36 amps maximum per resistor. This capacitative current varies linearly with the voltage along the strap, approaching zero at the short circuit. The Short Assembly, with differing strap design and reduced coupling, generates a similar level of current when operating at 50 kV. The inductively-driven current results partly from the inclination of the screen and is maximum at the current maximum in the strap near the short circuit.

The current distribution in the resistors has been determined calorimetrically and is found to vary weakly with distance along the strap, with a maximum between the short circuit and mid-point of 55 amps rms at 50 kV. The total inductively-driven current in the A2 screen elements will, on this basis, be similar to that in the central conductor.

5.6 *Manufacture*

Whilst the A2 antennae have no water cooling and thus no vacuum boundary, they are highly stressed assemblies and require careful control of quality during manufacture, in particular of the many different types of weld. Furthermore, the geometrical

design is highly intricate due to the lack of any symmetry in the shape of the antennae and to the convoluted construction. Extensive use of CAD has been required in the production of manufacturing drawings, and a wide range of jigs and tools necessary for the manufacture. Manufacture of the prototype unit is now proceeding.

6 Conclusion

Since the inception of the RF programme at JET in 1982, a series of antennae have been produced. Operation of these antenna on JET has led to the achievement of many milestones in coupled ICRF power and energy, in technical understanding of the operation of the antenna in a tokamak environment, and the demonstration of important new results using ICRF heating of a tokamak plasma. This paper has described the technical aspects of the antennae until recently operating in JET and the new antennae which are anticipated to be operating on the pumped divertor plasma after the present shutdown.

References

[1] Kaye A. S., Jacquinot J., Lallia P., Wade T., "Radio Frequency Heating System", Fusion Technology 11, 1, (1987)203-234.

[2] Walker C. I., Kaye A. S., Brinkschulte H., Horn R. A., Plancoulaine J., Sigourney D., Bevilacqua G., Anselmi F., "Design and Manufacture of Water-cooled Screens for JET ICRF Antennae", Fusion Technology (14th Symposium, Avignon, 1986) 807-817.

[3] Walker C. I., Brinkschulte H., Bures M., Dragomelo N., Coad J., Kaye A. S., Knowlton S., Plancoulaine J., "The JET ICRF Antenna Screen: Experience with

Actively Cooled Nickel Screens and Design of New Beryllium Screen", Fusion Technology (15th Symposium, Utrecht, 1988) Vol. I, 444-448.

[4] Wade T. J., Kaye A. S., Jacquinot J., "The Technology of the Upgraded JET ICRF Heating System", Fusion Technology (7th Topical Meeting, Rome, 1986) 10, 3, 1398-1403.

[5] Jacquinot J., Bures M. and the JET Team, "JET Results with both Fast and Lower Hybrid Waves and Consequences for Future Devices", Phys. Fluids (accepted for publication), 1992.

[6] Bures M., Jacquinot J., Lawson K., Stamp M., Summers H., D'Ippolito D., Myra J., "Impurity Released from the ICRF Antenna Screens on JET", Plasma Physics and Controlled Fusion, 33, 8 (1991) 937-967.

[7] D'Ippolito D. A., Myra J. R., Bures M., Jacquinot J., "A Model of Sheath-driven Impurity Production by ICRF Antennae", Plasma Physics and Controlled Fusion, 33, 6, (1991) 607-641.

[8] Bures M., Jacquinot J., Stamp M., Summers D., Start D. F. H., Wade T., D'Ippolito D., Myra,J., "Assessment of Beryllium Faraday Screens on the JET ICRF Antennae", Nuclear Fusion (Accepted for Publication).

[9] Tubbing B., Jacquinot J., Stork D., Tanga A., "H-modes in JET with Ion Cyclotron Resonance Heating Alone", Nuclear Fusion 29, 11 (1989) 1953-1957

[10] Bhatnagar V., Jacquinot J., Tubbing B., Stork D., Tanga A., Balet B., Bosia G., Bures M., Campbell D., Clement S., Hatayama A., Lawson K., Tibone F., Start D. F. H.,

"ICRF Produced H-modes in the JET Tokamak", Plasma Physics and Controlled Fusion 33, 2 (1991) 99-121.

[11] Tubbing B., et al., "H-mode Confinement in JET with Enhanced Performance by Pellet Density Profiles", Nuclear Fusion 31, 5 (1991) 839-850.

[12] Start D. F. H., et al., "Fast Wave Heating and Current Drive in JET: Present Results and Future Plans", Proc. IAEA Tech. Committee on Fast Wave Current Drive in Reactor Scale Plasmas, Arles, Sept 1991, 226-243.

[13] Jacquinot J. and the JET Team, "Heating, Current Drive and Confinement Physics with the JET ICRH and LHCD Systems", Plasma Physics and Controlled Fusion, 33, 13 (1991) 1657-1675.

[14] Gormezano C., Brusati M., Ekedahl A., Froissard P., Jacquinot J., Rimini F., "Synergistic Effects Between Lower Hybrid and Fast Magnetosonic Waves in JET", Proc. IAEA Tech. Committee on Fast Wave Current Drive in Reactor Scale Plasmas, Arles, Sept. 1991, 244-259.

[15] Huguet M. and the JET Team, "JET Status and Prospects", Fusion Engineering (14th Symposium, San Diego, 1991), Vol. I, 162-167.

[16] Bhatnagar V., Jacquinot J., Kaye A. S., "JET ICRH Antenna for the Pumped Divertor Geometry", JET Report JET-R(89)16.

[17] Lobel R., Bhatnagar V., Jacquinot J., Kaye A. S., Panissié H., Rebut P-H., "ICRF Antenna for the JET Pumped Divertor Configuration", Fusion Technology (16th Symposium, London, 1990), Vol. I, 73-78.

[18] Walker C. I., Kaye A. S., Horn R. A., Mazza F., "Non-evaporable Getter Pumping for JET ICRF Antenna", Fusion Technology (15th Symposium, Utrecht, 1988), Vol. I, 815-820.

[19] Kaye A. S., Anderson R., Arbez J., Bosia G., Beaumont B., Bures M., Jacquinot J., Lallia P., Plancoulaine J., Sand F., Schmid M., Wade T., Walker C., "Engineering Design and Preliminary Performance of the JET ICRF System", Fusion Engineering (11th IEEE Symposium, Austin, 1985), Vol. II, 1204-1209.

[20] Noterdaeme J-M., Ryter R., Söll M., et al., "The Role of the Faraday Screen in ICRF Antennas: Comparison of an Optically Open and an Optically Closed Screen on ASDEX", in Controlled Fusion and Plasma Heating (13th EPS, Schliersee, 1986), 137-140.

[21] Wade T. J., Jacquinot J., Bosia G., Sibley A., Schmid M., "High Power (22 MW) ICRH at JET and Development for Next Step Devices", Fusion Engineering (14th Symposium, San Diego, 1991), Vol II, 902-907.

[22] Bhatnagar V. P., Jacquinot J., Start D. F. H., "Fast Wave Current Drive Efficiency Calculations for JET A2 Antennas", Proc. IAEA Tech. Committee on Fast Wave Current Drive in Reactor Scale Plasmas, Arles, Sept 1991, 110-120.

[23] Bhatnagar V. P., Jacquinot J., Gormezano C., Start D. F H. and the JET Team, "ICRF Heating and Synergistic LH and Fast Wave Current Drive in JET", Radio Frequency Power in Plasmas (Charleston, 1991) AIP Conference Proc. 244, 115-124.

TABLE 1 : Specification of the JET ICRF System

	Original	Present (Be screen)
Coupled power (MW)	15	20
No of antennae	10	8
No of amplifiers	20	16
Unit power (MW)	1.5	2
Frequency range (MHz)	25-55	25 - 55
Pulse length (s)	20	20
Duty cycle	1:30	1:60
Neutron fluence at window (cm^{-2})	10^{17}	10^{17}
Remote handling requirement	all antenna systems	
Design voltage (kV peak)	50	50
Toroidal locations	1D,2B,3D,4B,5D,6B,7D,8B	

TABLE 2 : Specification of the A2 Antennae

Coupled power	24 MW
No of antennae	8
Toroidal locations	1D,2B,2D,3B,5D,6B,6D,7B
Pulse length	20 s
Duty cycle	1:60
Remote handling	Window only
Design voltage	42 kV peak

TABLE 3: Ceramic Resistors: Disruption Simulation and RF Test Results

TYPE OF TEST	PERFORMANCE ACHIEVED TO DATE	REQUIRED PERFORMANCE
RF Test Bed Subjects a pair of resistors to 20 s pulses at 25 - 55 MHz. Resistors operate at 300 - 600 C at 1.10^{-6} mbar	65 Amps rms for 20 s pulses at 48 MHz with 10:1 duty cycle. Temp rise during pulse 300 C.	60 Amp rms. 20 s pulses 60:1 duty
Disruption Simulation Test Bed Subjects individual resistors mounted in A2-style jigs to current pulses of up to 1500 Amps peak, 10 - 20 millisec variable duration and shape.	680 Amps peak during quasi-sine wave pulses of 13 msec duration (210 joules deposited energy)	340 Amp 83 joules

TABLE 4:

Model	λ/4 Resonance	λ/2 Resonance
Short Assembly	38.8 MHz	58 MHz
Low power model	41.5 MHz	49.4 MHz

TABLE 5: Short Assembly Test Conditions and Equipment

Test Vessel internal dimensions	2.8 m height x 1.5 m diameter
Vessel temperature: Bake-out	300 C
Testing	200 C
Vessel pumping speed:	3500 l/s
Vacuum Transmission Line Pressure	$< 5.10^{-5}$ mbar
Diagnostics	Infrared Thermometry Gas Analysis Arc trips on generator with 20 μsecs response time
Pressurised Transmission Lines	30 Ω, 225 mm OD purged with dry air (< -30 C dew point) at 3 bar
Matching Network:	Double stubs 25 m from the antenna

TABLE 6: Short Assembly RF Test Results

Test Parameter	Measured or Achieved Value
Test Frequencies	55 42 and 24 <Hz (approx)
RF Pulse length	20 s
RF Peak Line Voltage for reliable operation[1]	50 kV at all test frequencies
Maximum Line Voltage Achieved	60 kV at 42 MHz with 100 ms pulses
Peak Line Current for reliable operation[1]	1 kA at all test frequencies
Maximum duty cycle[2]	20:1
Peak voltage with Open Circuit Strap[3]	49 kV at 28 MHz

1. Typically achievable with no arcing after 4 - 8 hours of multipactor and short pulse conditioning.
2. Limited by temperature rise in the Pressurised Transmission Line
3. With gap to screen elements increase to 18 mm; 40 kV with standard 12 mm gap.

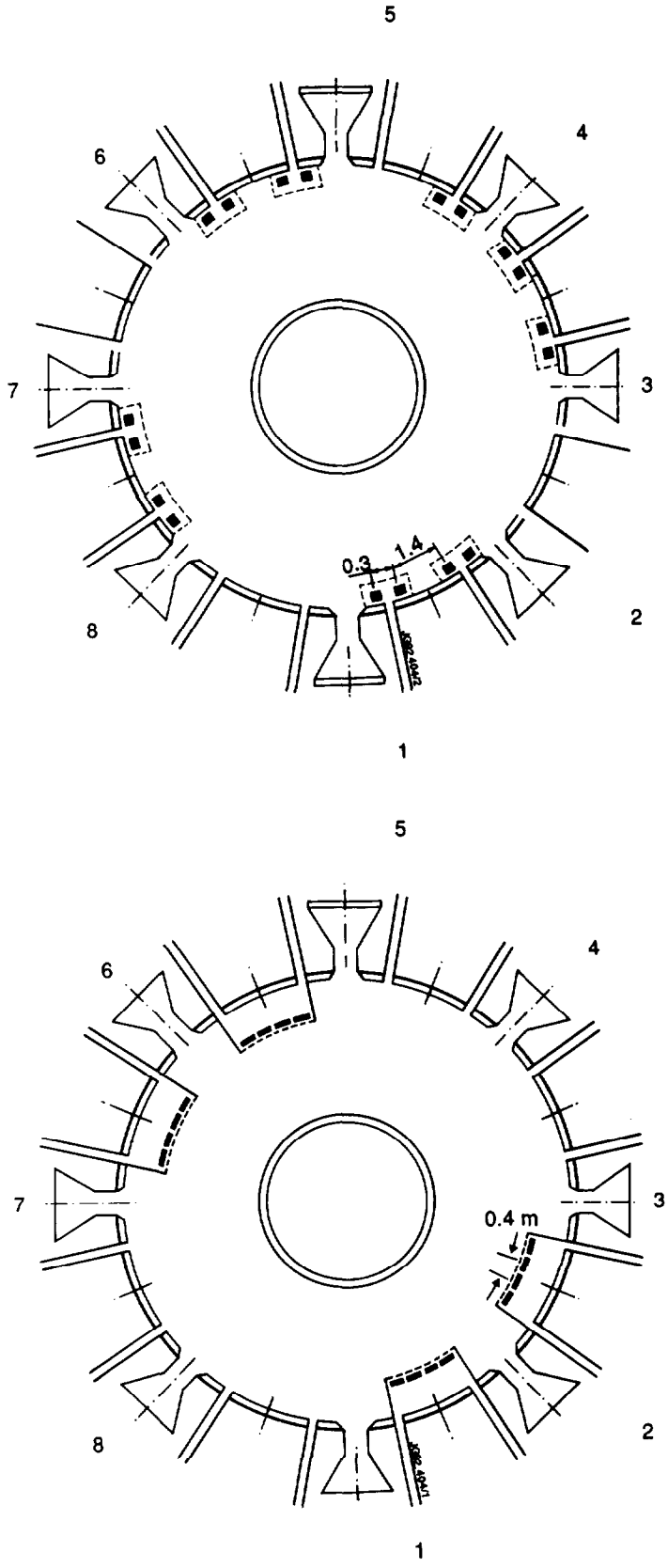

Fig 1: Layout of the ICRF Antennae in the torus:

a) A1 Antennae

b) A2 Antennae

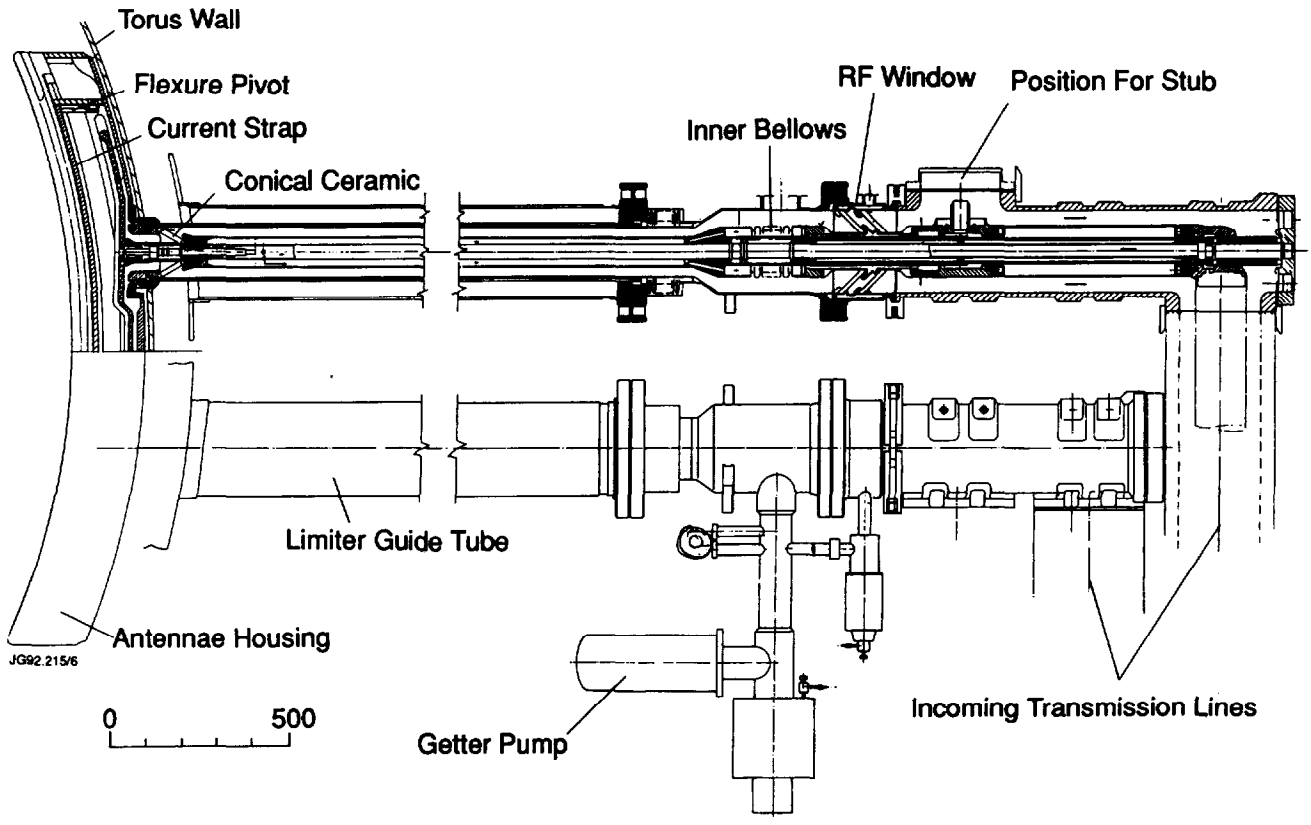

Fig 2: **A vertical section through the A1 ICRF antenna showing both the antenna and the vacuum transmission line.**

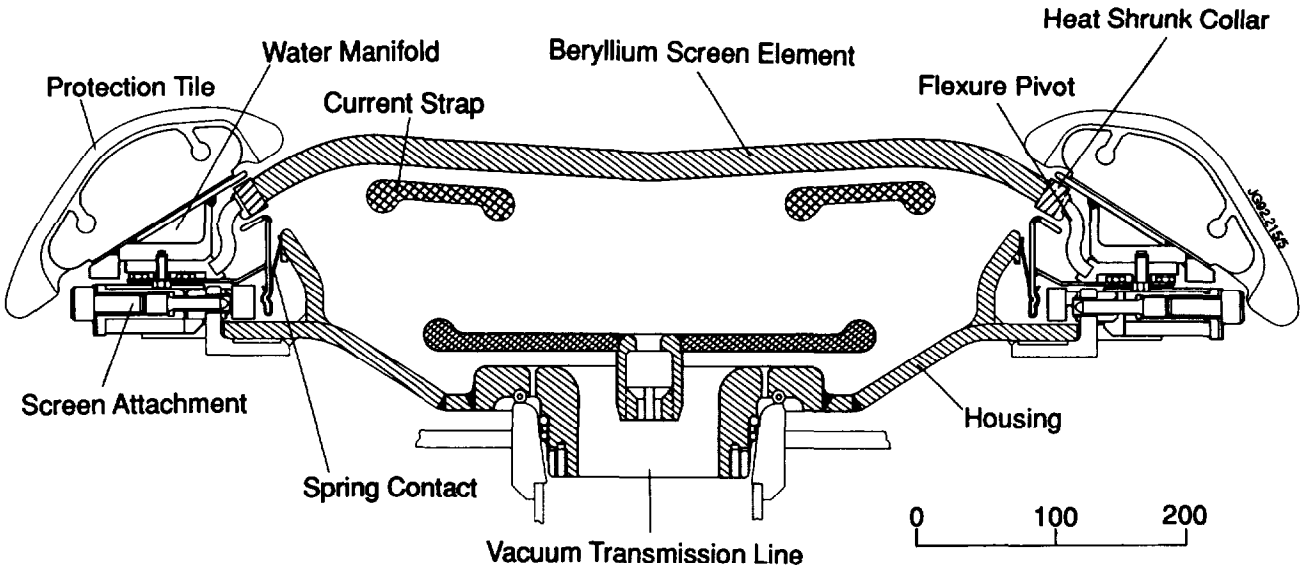

Fig 3: **An horizontal section through the A1 antenna with beryllium screen.**

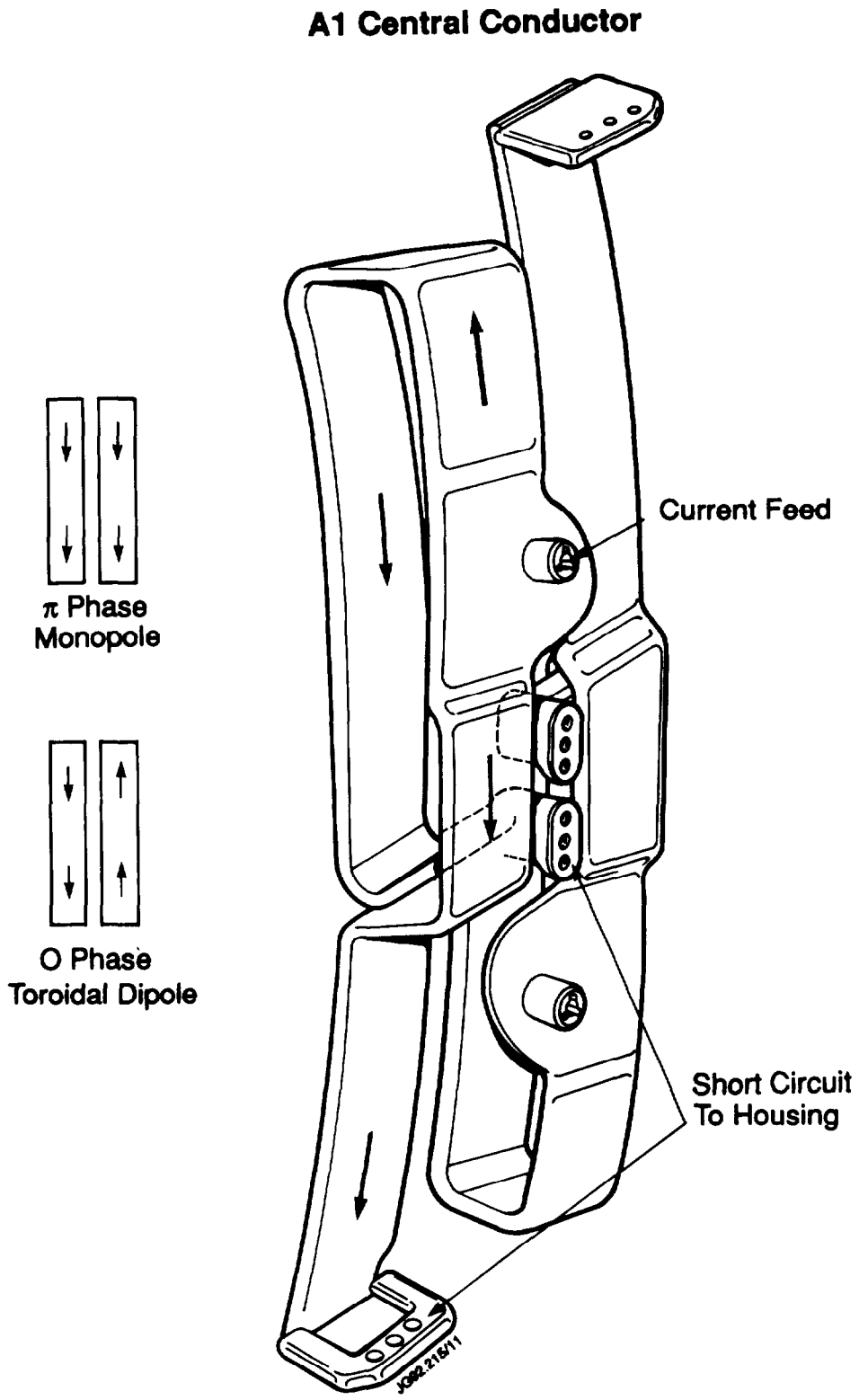

Fig 4: The A1 current straps viewed from outside the torus. Each of the two straps per antenna is fed by a separate tetrode. The phase difference between tetrodes is normally 0 or π.

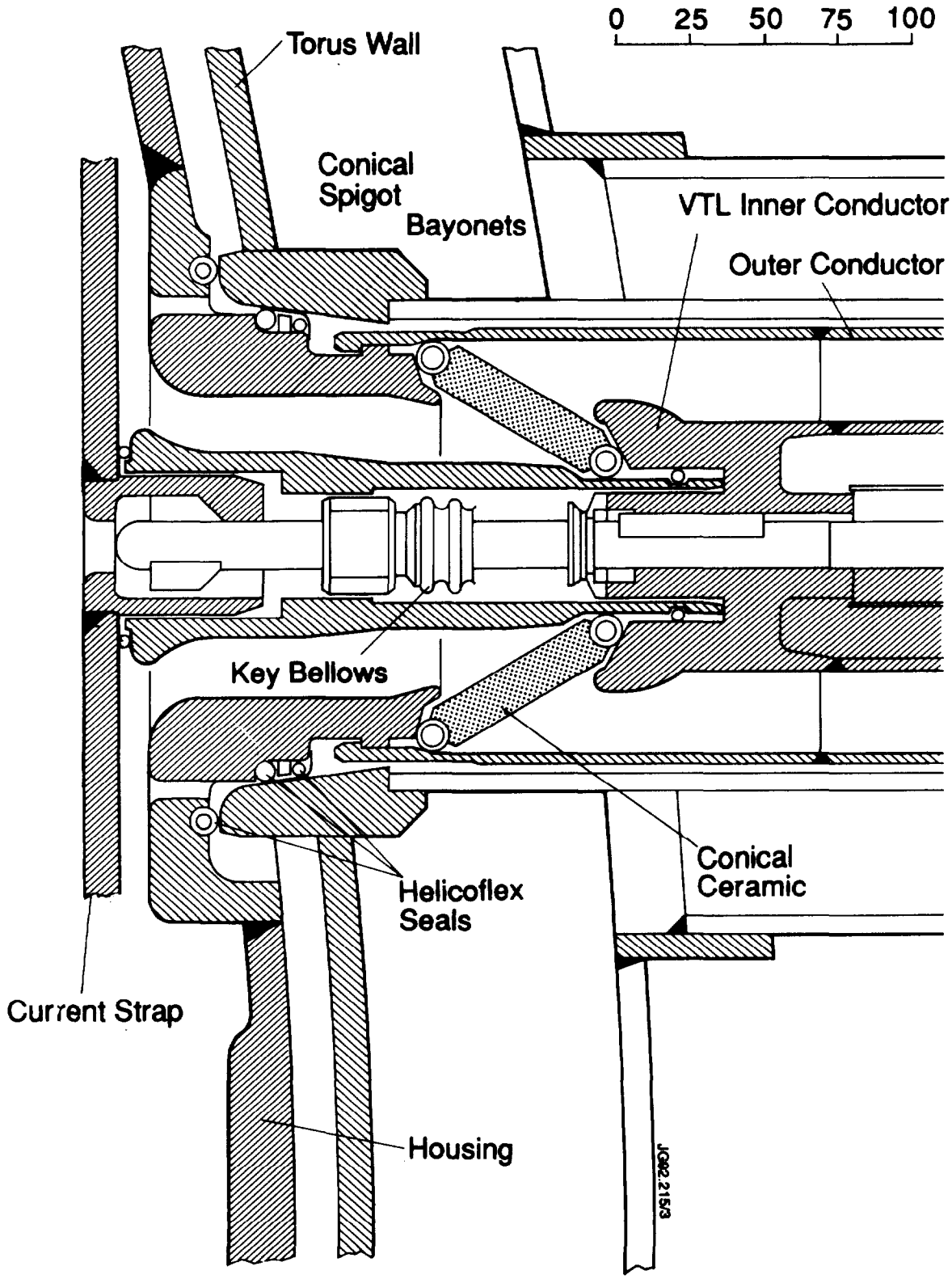

Fig 5: One of the spring contacts connecting the screen to the housing to establish RF contact whilst restricting the disruption-induced eddy currents.

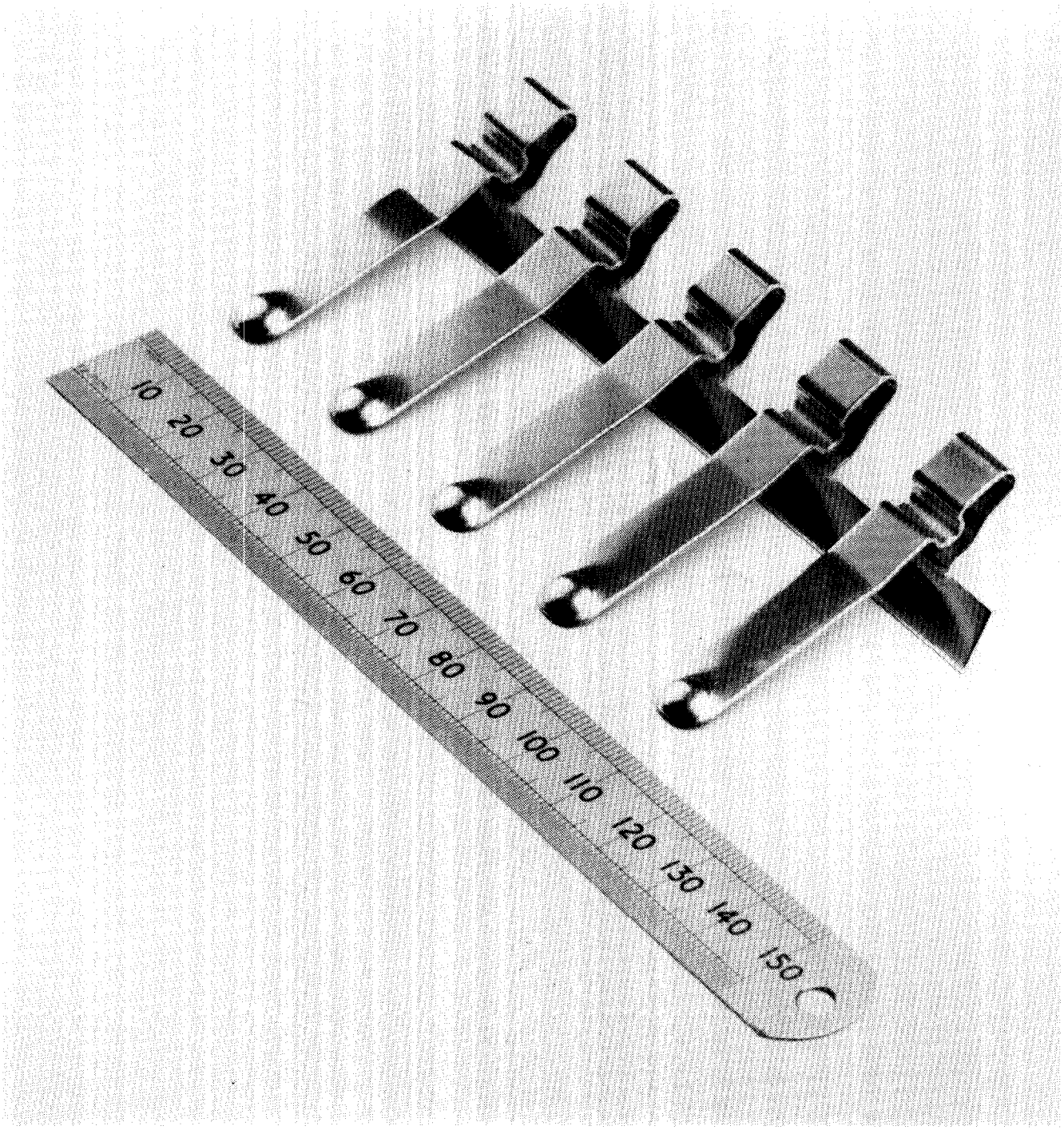

Fig 6: A detailed section of the antenna/vacuum transmission line/torus wall interface. Helicoflex seals are used both to establish RF contact on current-carrying surface and for compliant support on the torus wall.

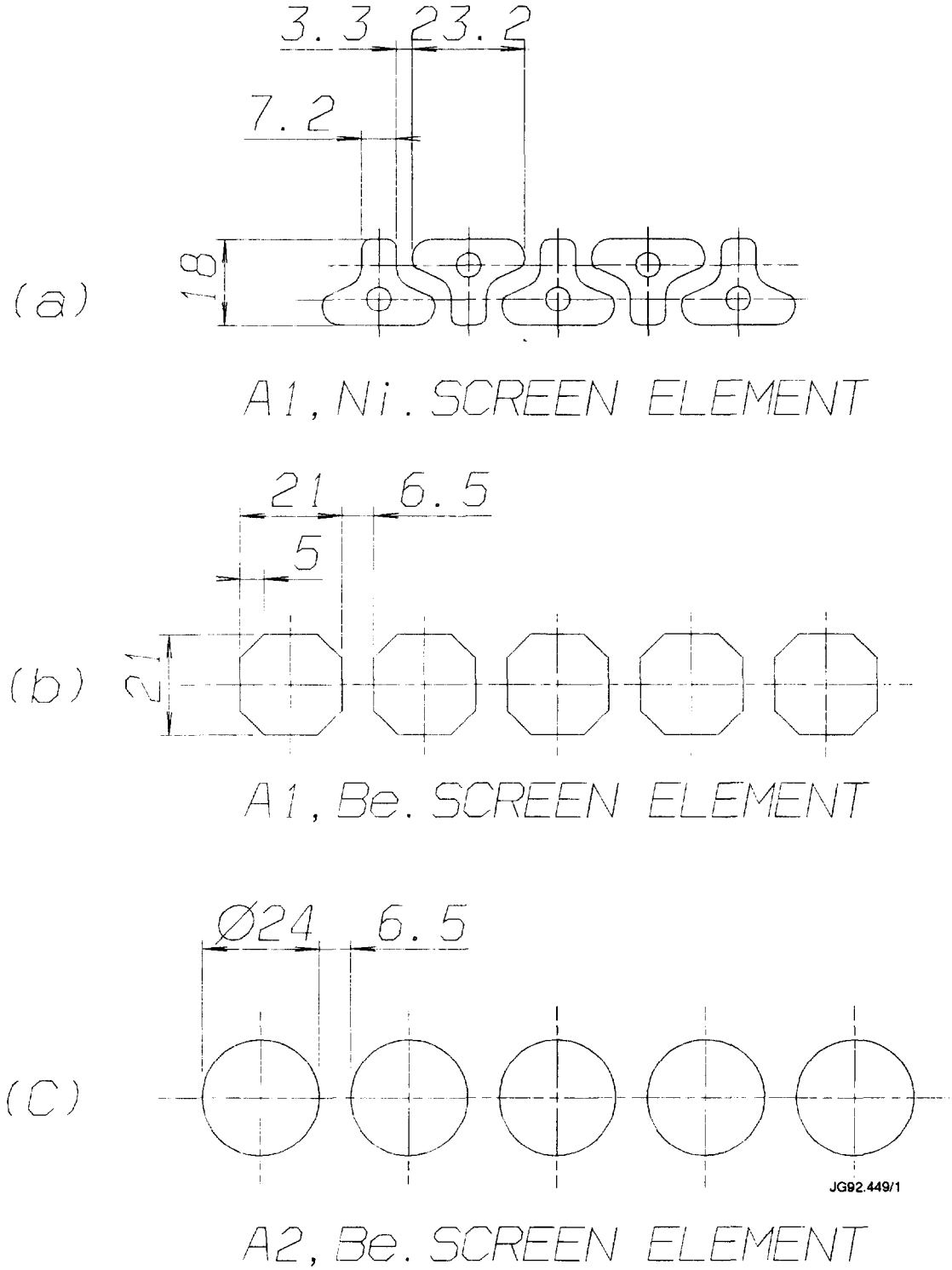

Fig 7: Sections through the screen elements of the various JET screens:

a) A1 nickel screen

b) A1 beryllium screen

c) A2 beryllium screen

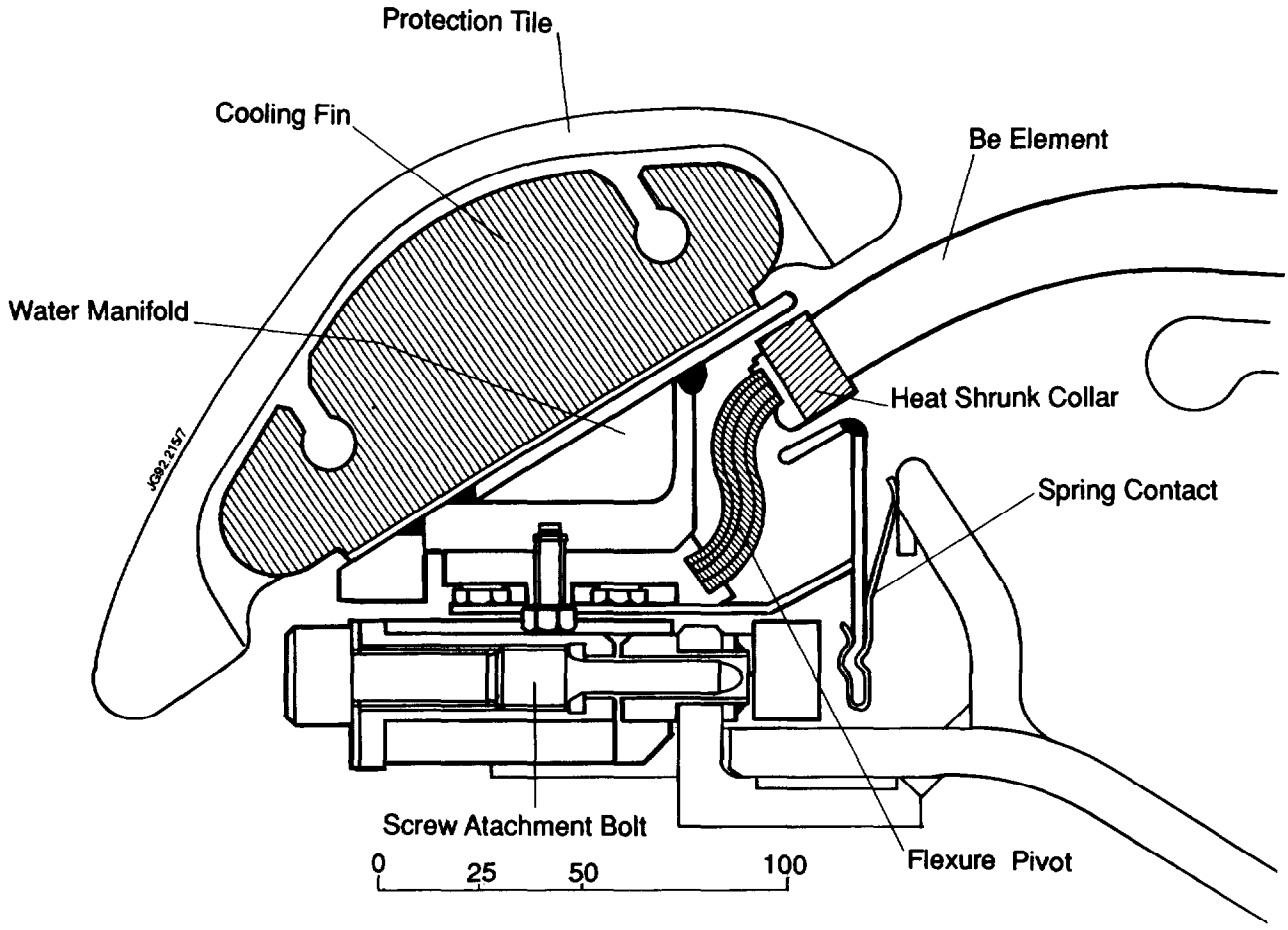

Fig 8: A detailed section of the attachment of the beryllium elements to the water manifold and the housing. The flexure pivot comprises 16 foils welded into end fittings.

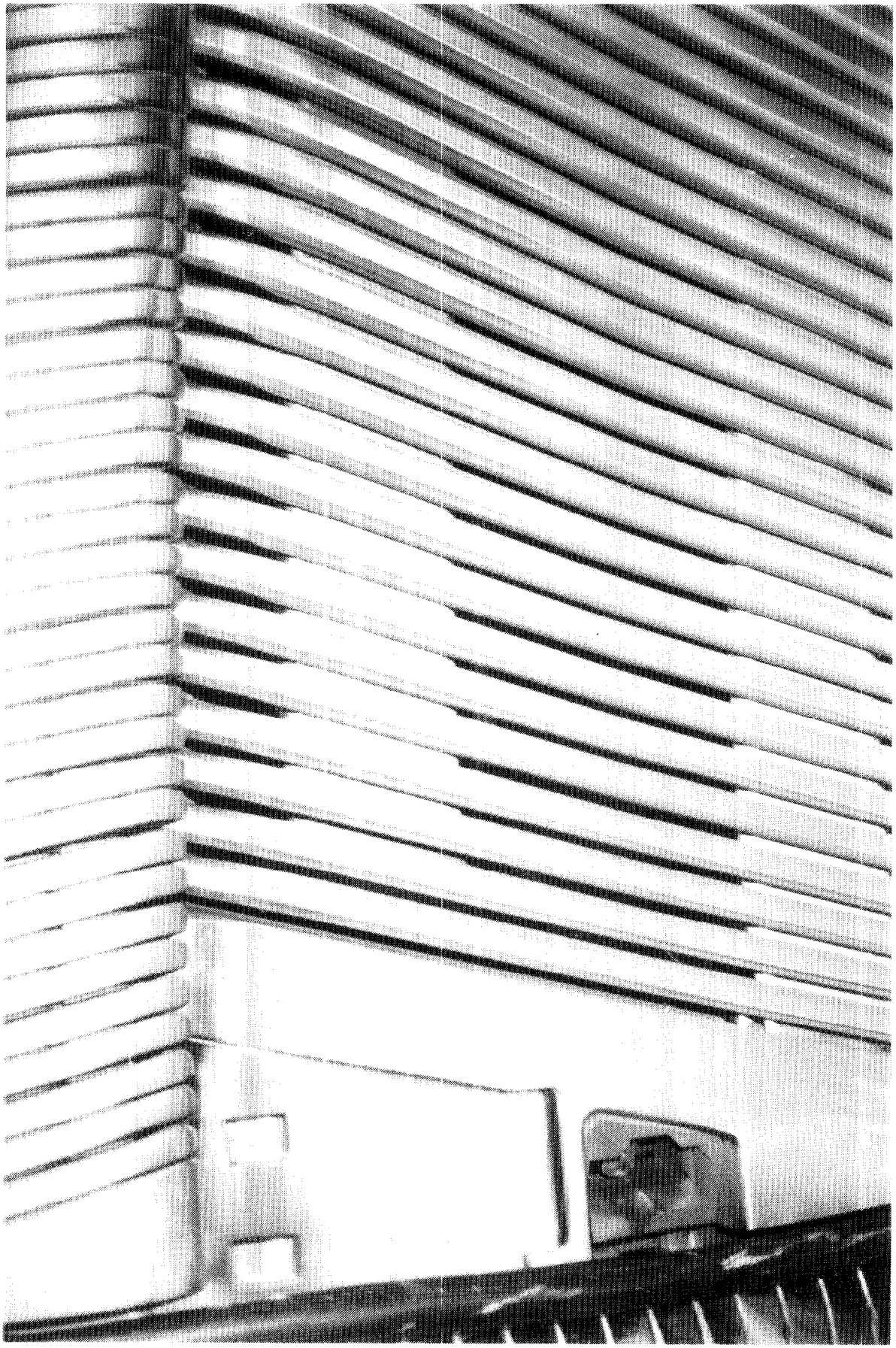

Fig 9: A photograph of the A1 antenna with beryllium screen inside the torus.

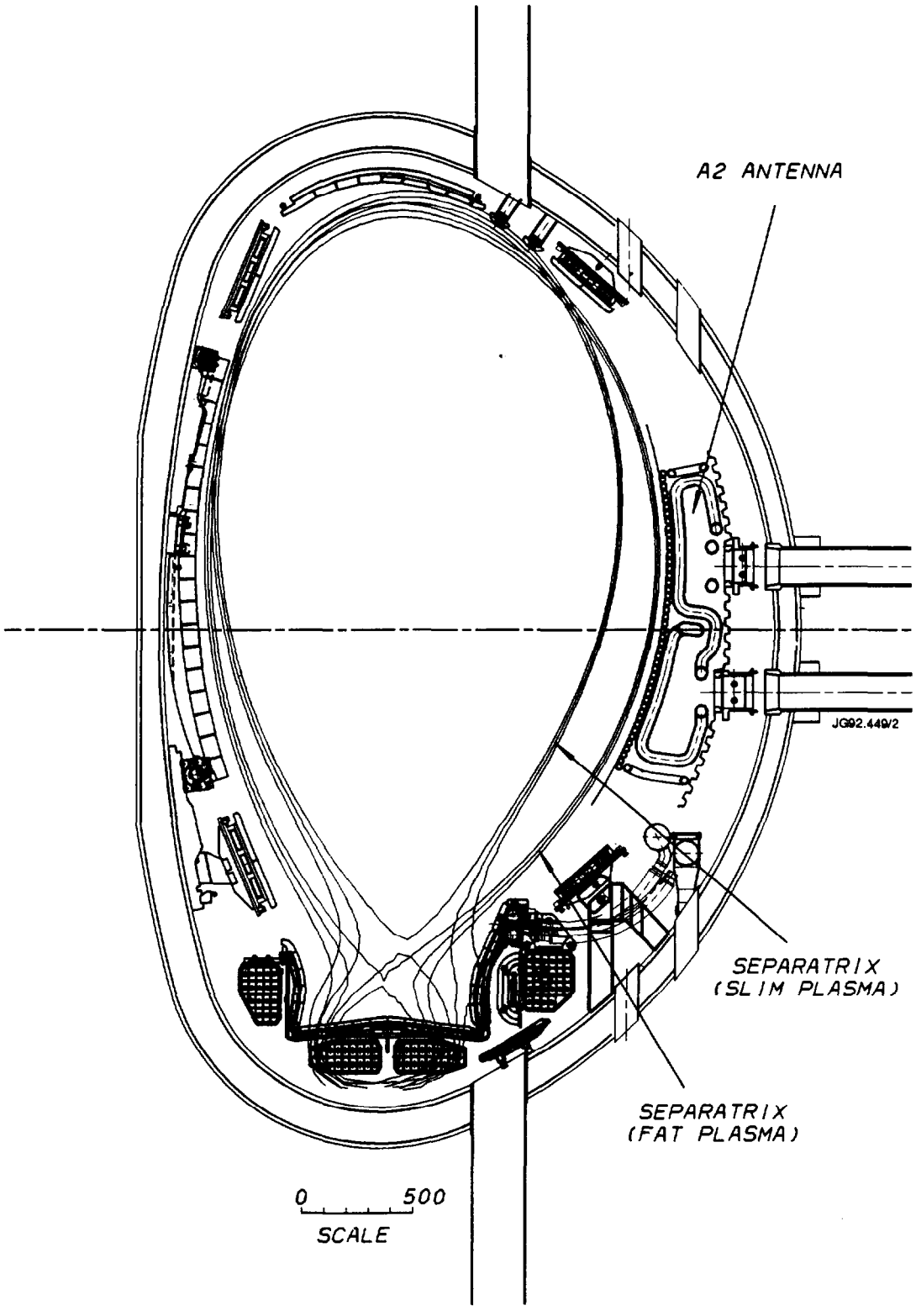

Fig 10: A section through the JET torus in the new pumped divertor configuration, showing the A2 antenna positioned to match the fat plasma. Two discrete plasma configurations (fat and slim) are anticipated for this phase.

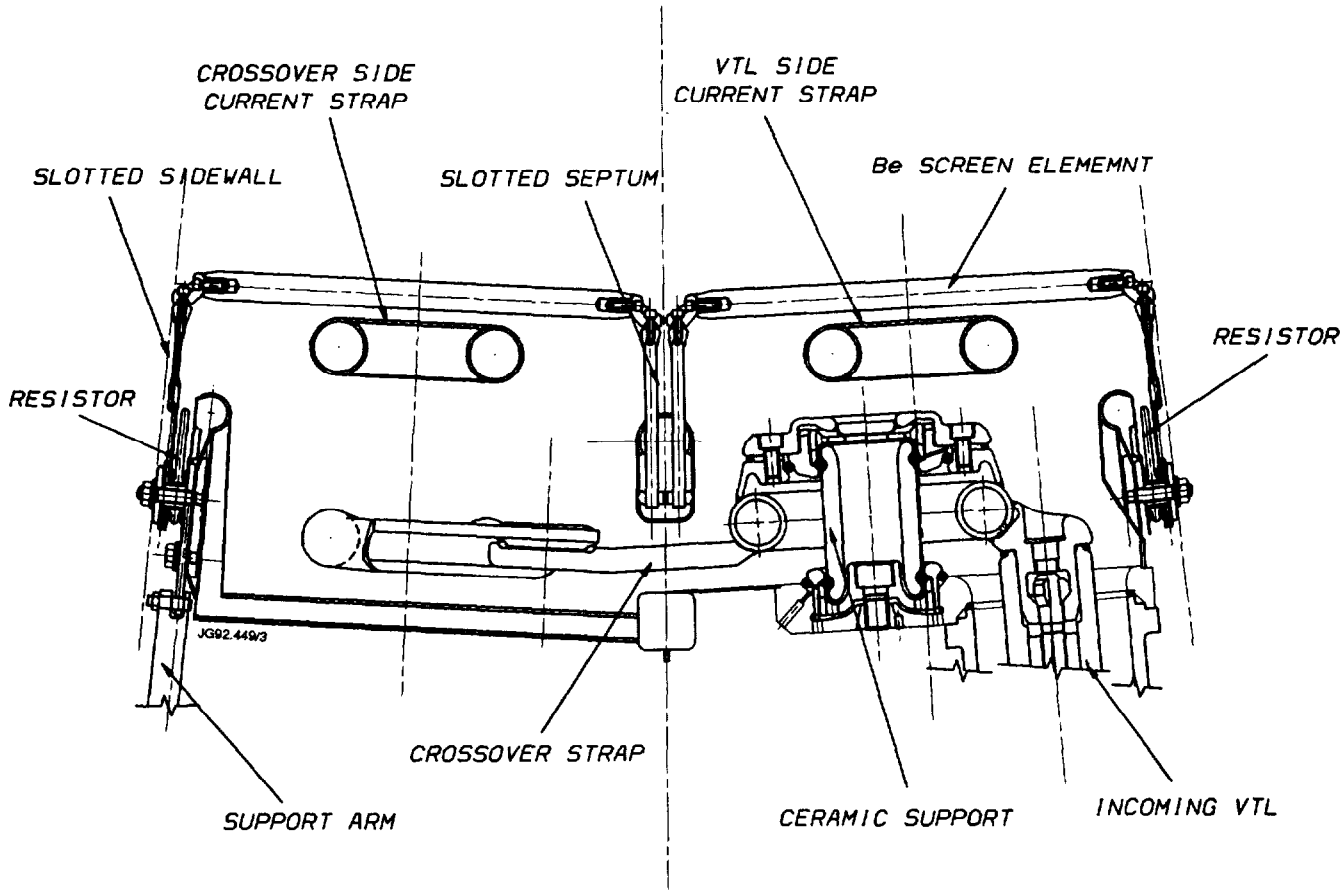

Fig 11: An horizontal section through the A2 antenna showing the general layout and the ceramic support for the current strap.

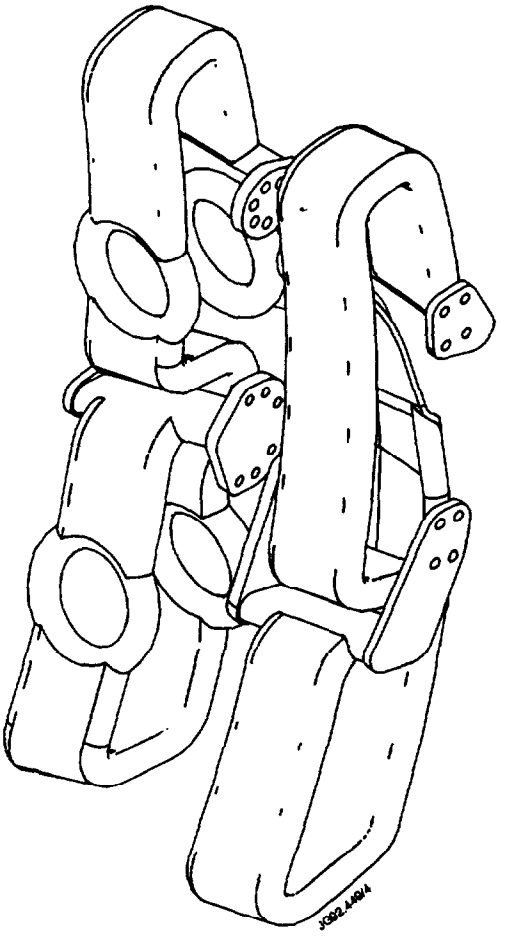

Fig 12: The current straps on the A2 antenna. The circular holes allow in-situ replacement of the ceramic supports.

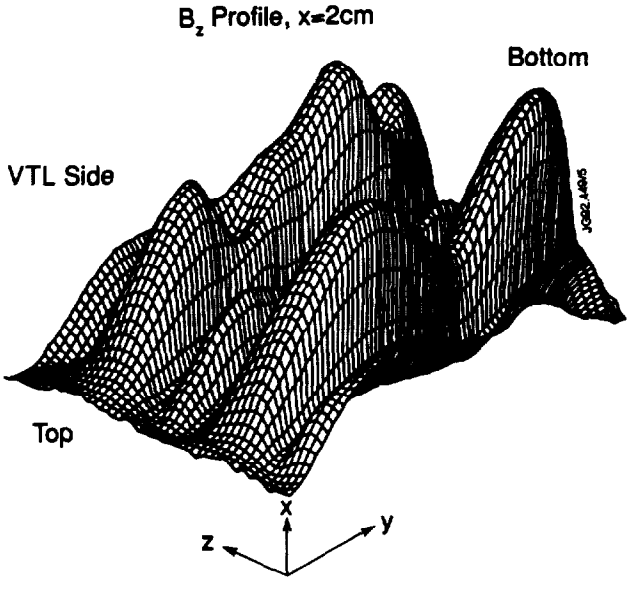

Fig 13: Typical measured distribution of the toroidal component of the RF magnetic field measured in front of the screen on the A2 flat model. (Courtesy of Oak Ridge National Laboratory).

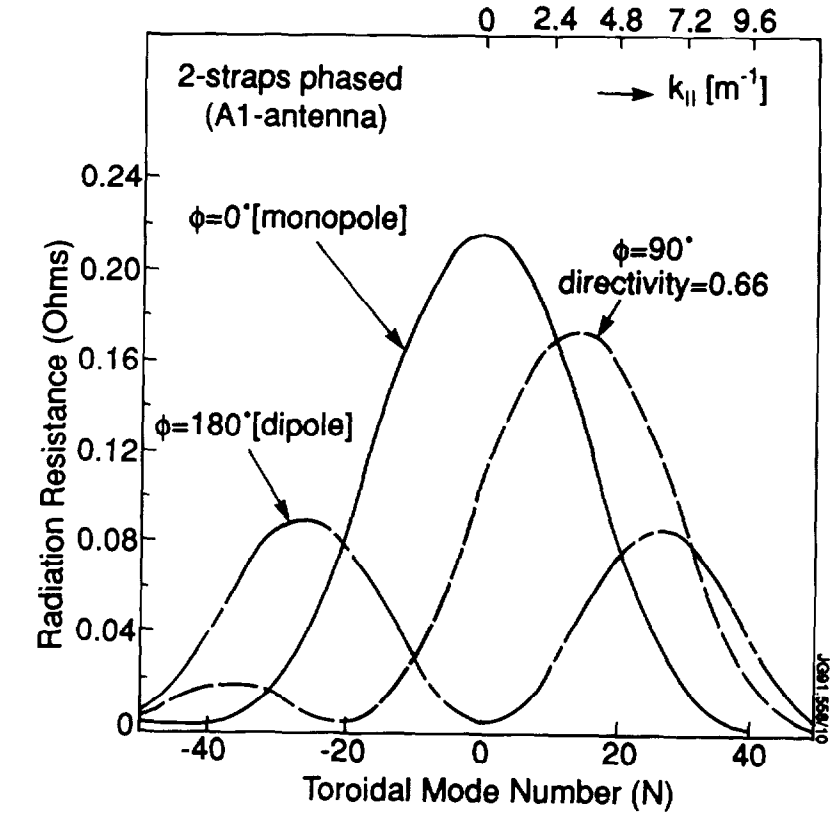

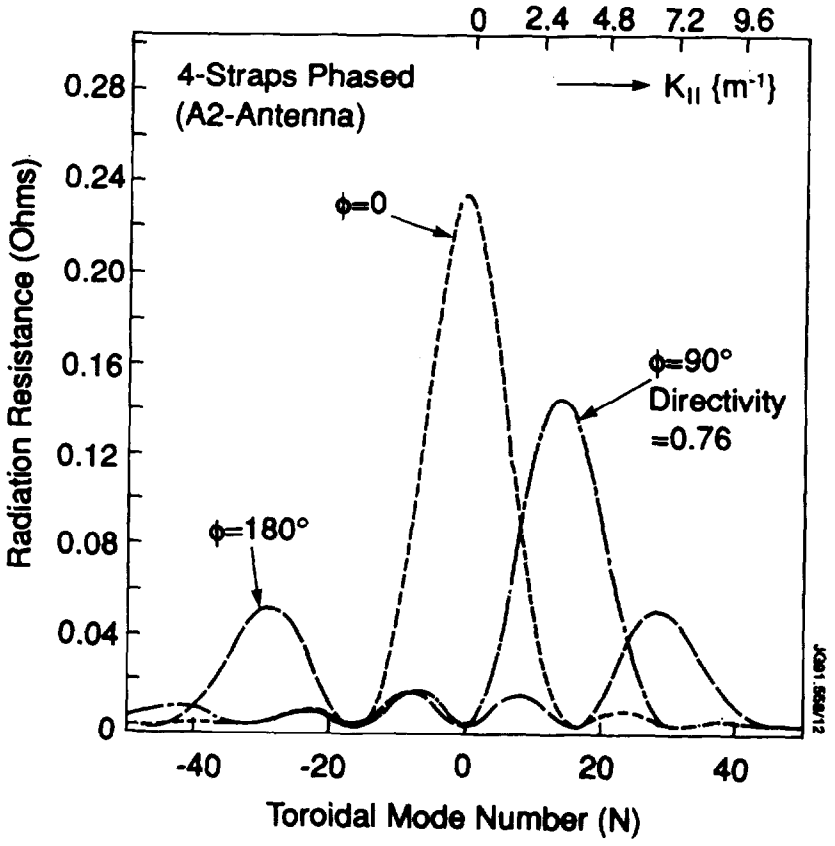

Fig 14: Typical computed spectra and directivities at 0°, 90° and 180° phase shift (ϕ):

a) A1 antenna, 2 current straps

b) A2 antenna, 4 current straps

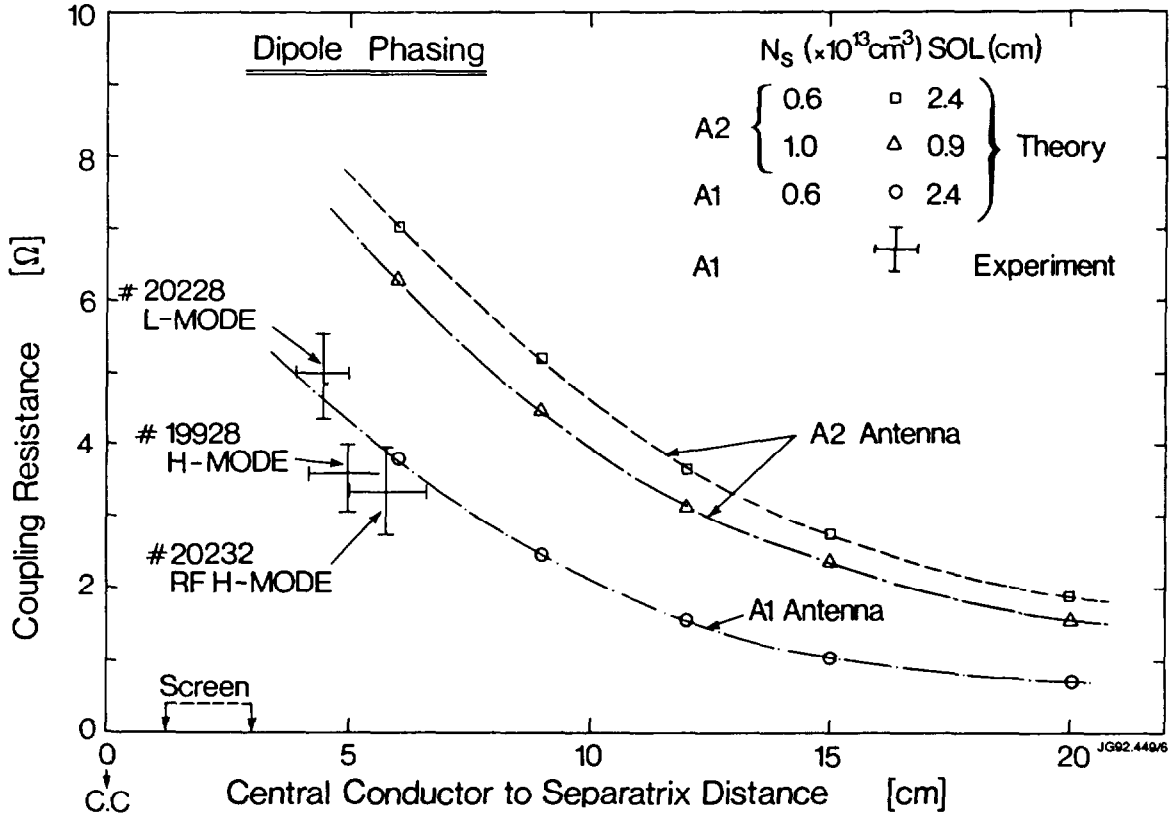

Fig 15: Computed coupling resistances for the A1 and A2 antennae as a function of the edge density (Ns) and scrape-off layer thickness (SOL). Typical measured data for the A1 antennae are also shown.

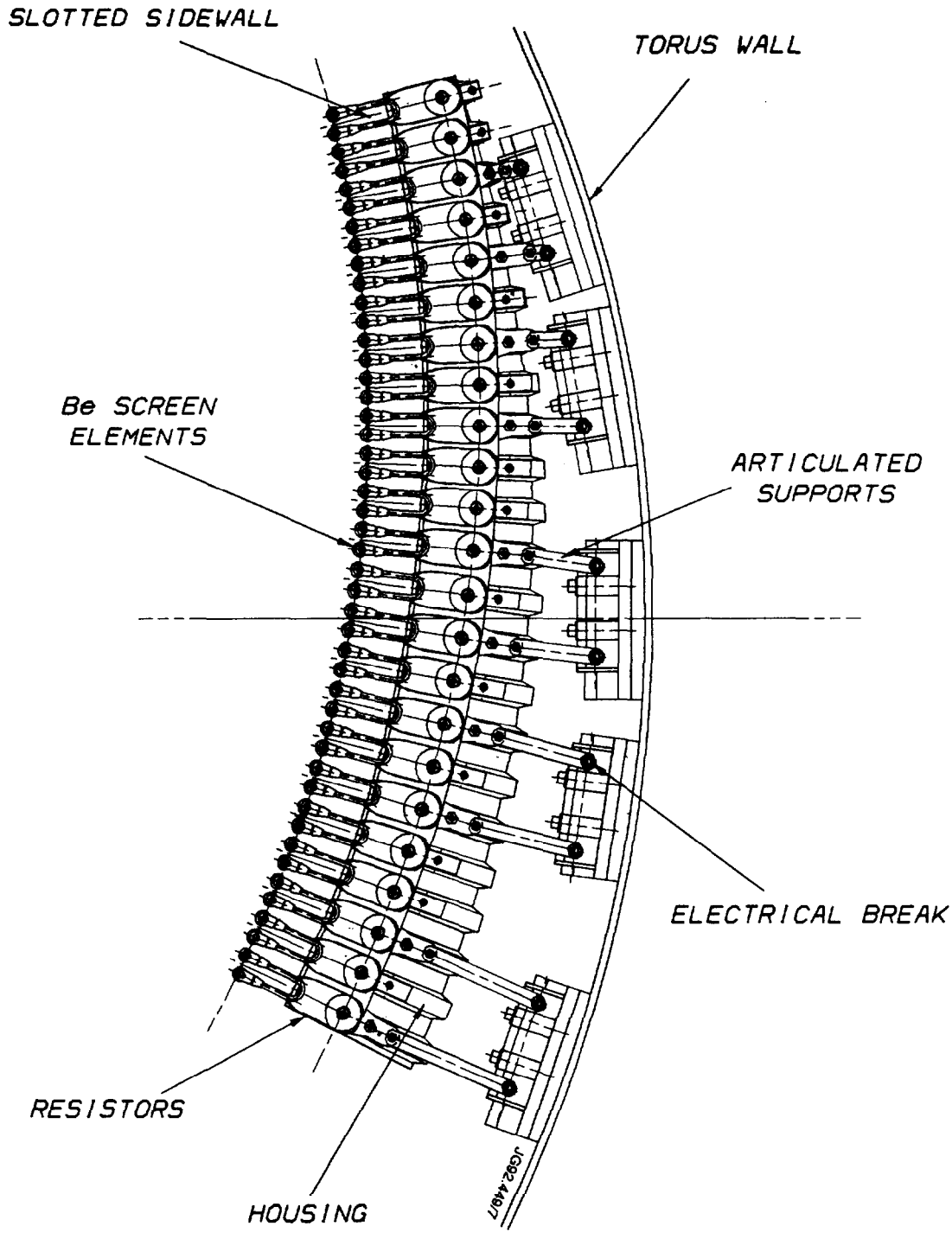

Fig 16: A view of one side of the A2 antenna, showing the slotted side-wall, resistor layout, corrugated antenna back-wall and the articulated supports to the torus.

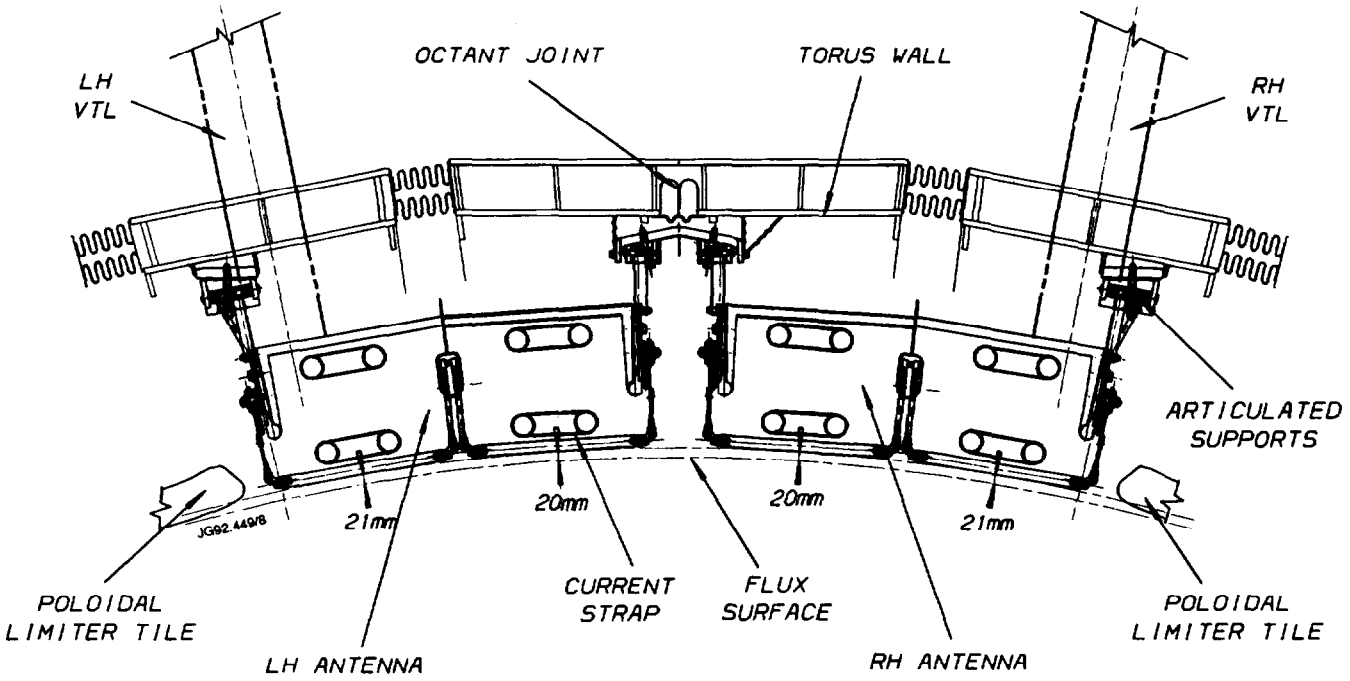

Fig 17: An horizontal section through one of the four pairs of A2 antennae in the torus. The current straps are at nearly constant pitch and sidewalls slotted to enhance the launched spectrum. Poloidal limiters protect the antenna sides.

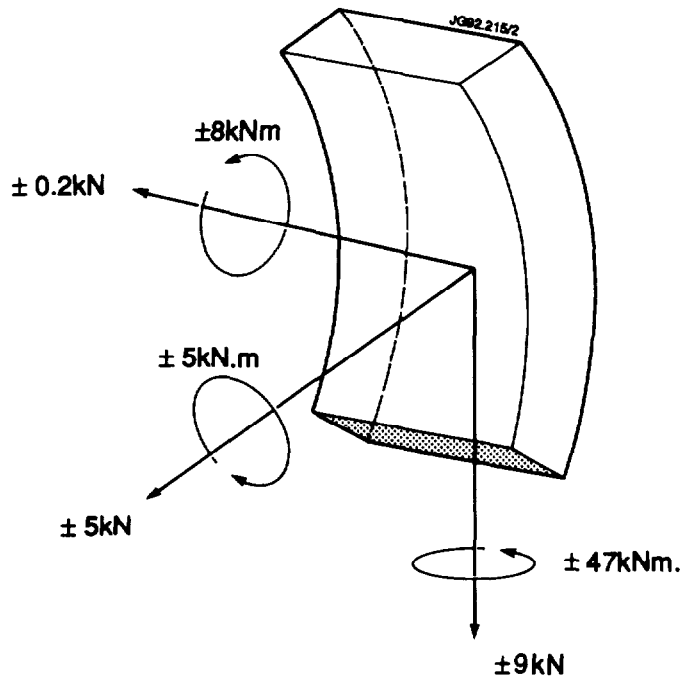

$\dot{B}_v$=120 Tesla / Sec
$\dot{B}_r$=150 Tesla / Sec

Fig 18: A summary of the forces appearing on the A2 antenna during a disruption.

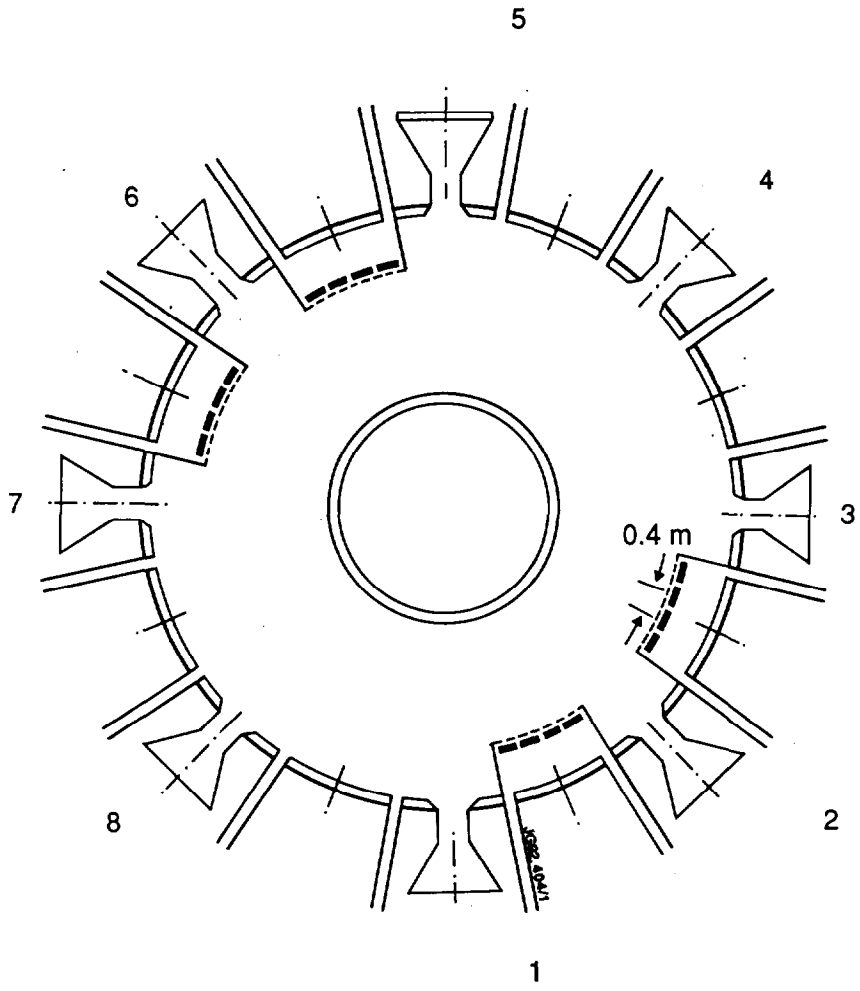

Fig 1(b)

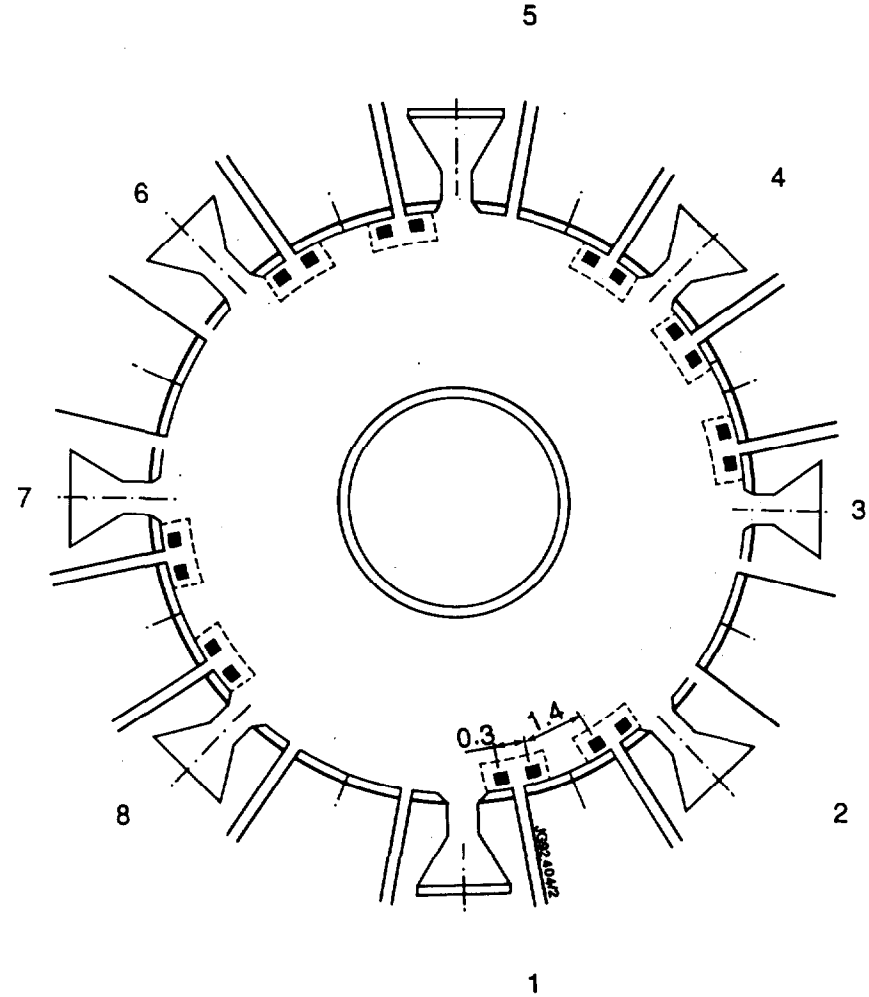

Fig 1(a)

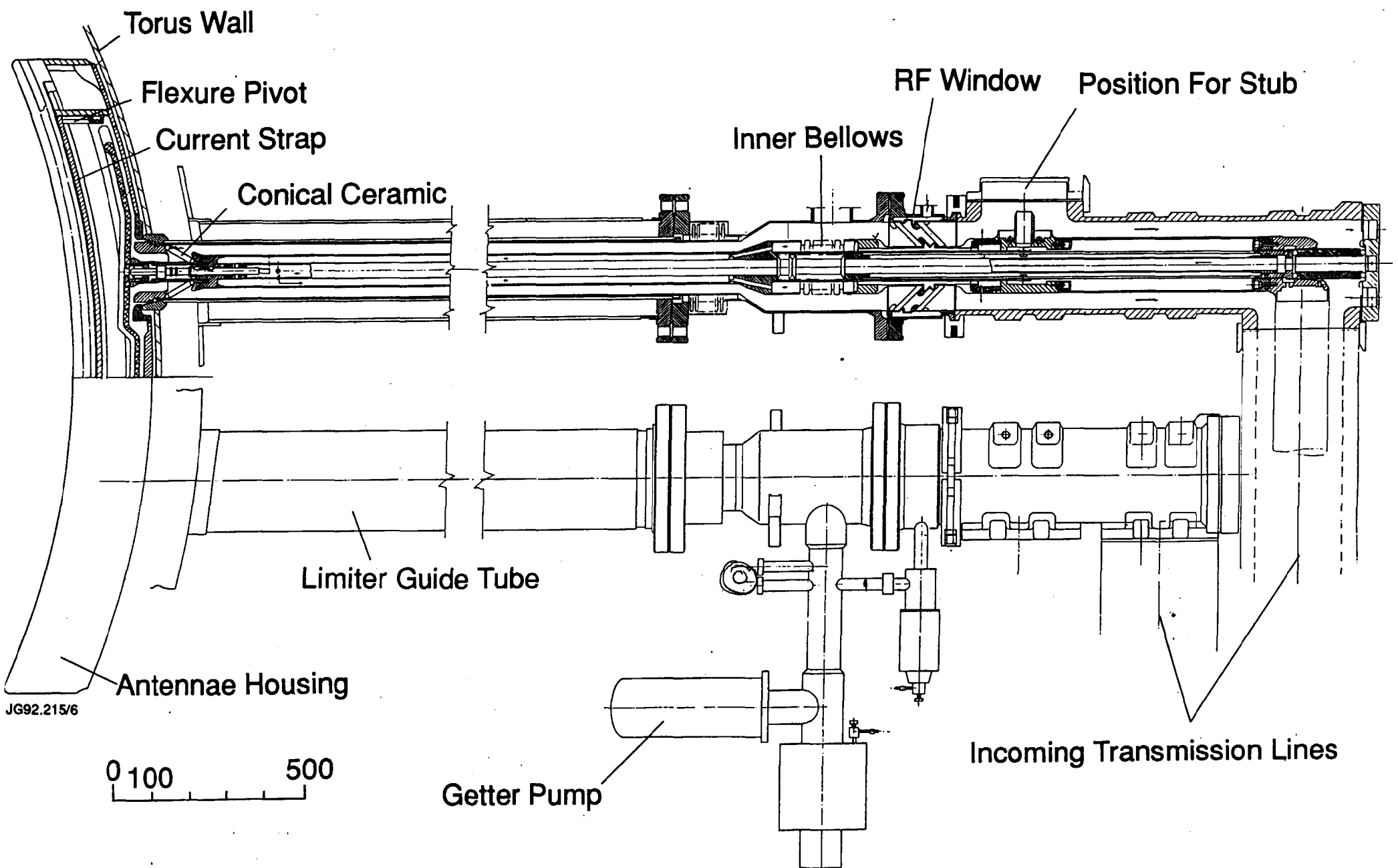
Torus Wall
Flexure Pivot
Current Strap
Conical Ceramic
RF Window
Position For Stub
Inner Bellows
Limiter Guide Tube
Antennae Housing
JG92.215/6
0 100 500
Getter Pump
Incoming Transmission Lines

Fig 2

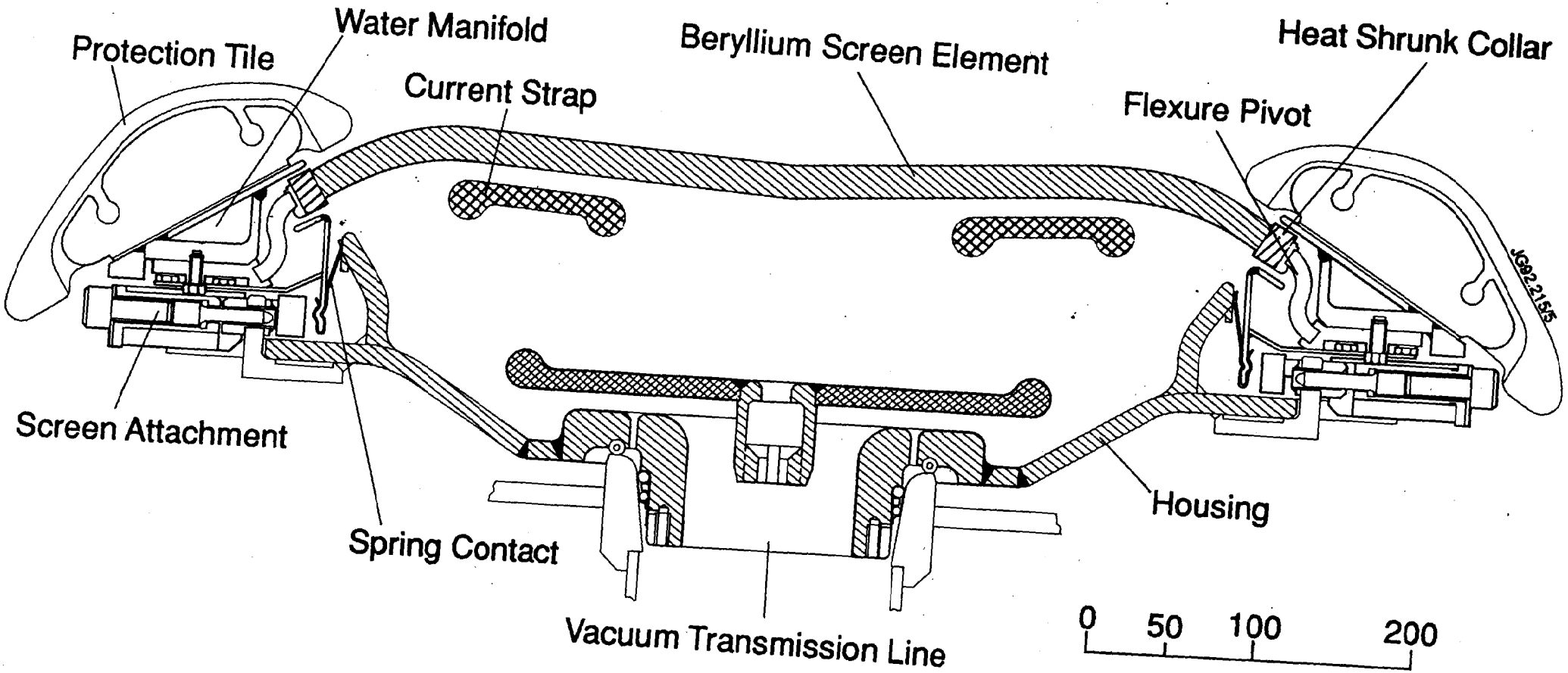
Protection Tile
Water Manifold
Current Strap
Beryllium Screen Element
Heat Shrunk Collar
Flexure Pivot
JG92.215-5
Screen Attachment
Spring Contact
Housing
Vacuum Transmission Line
0
50
100
200

Fig 3.

A1 Central Conductor

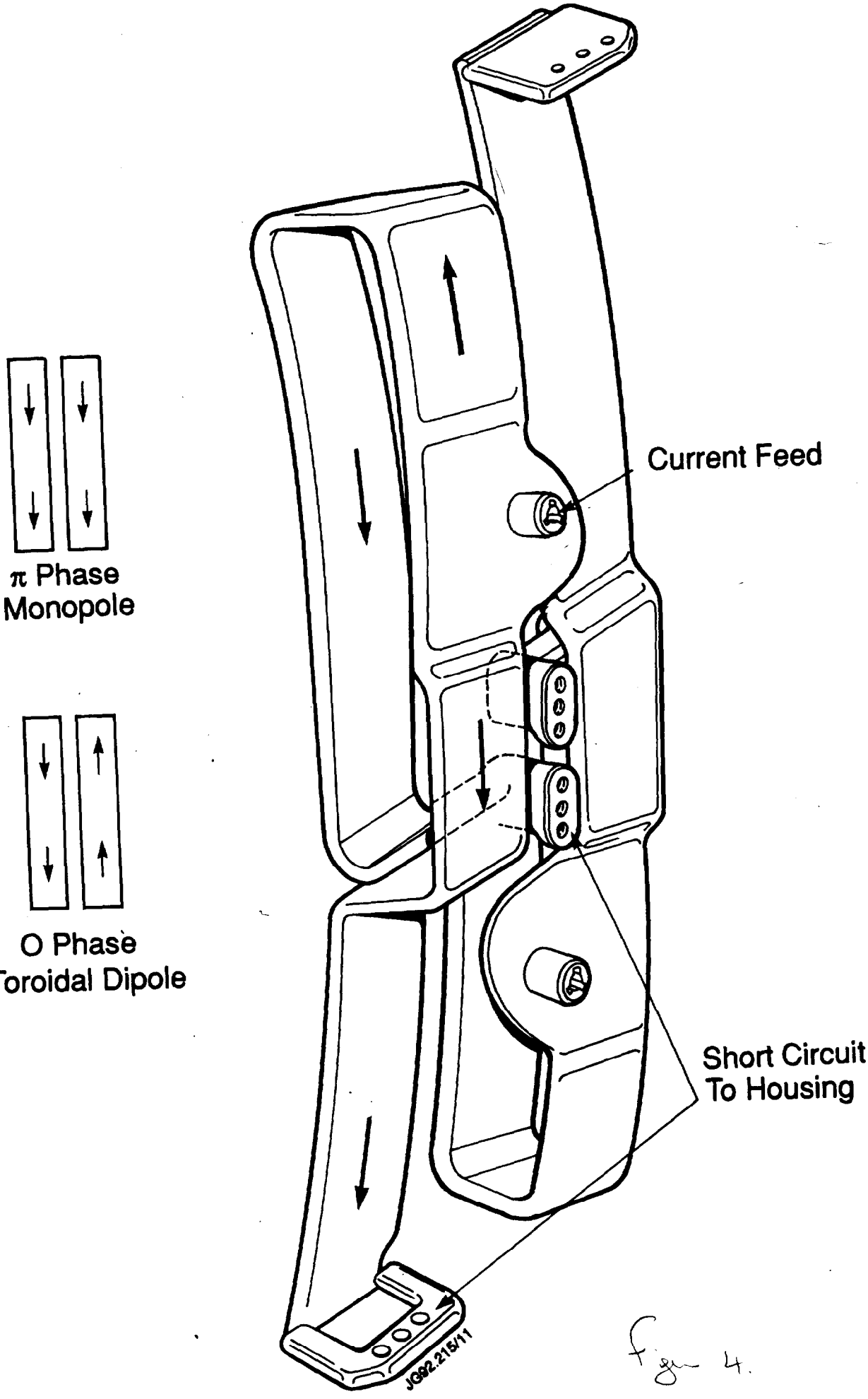

fig 4.

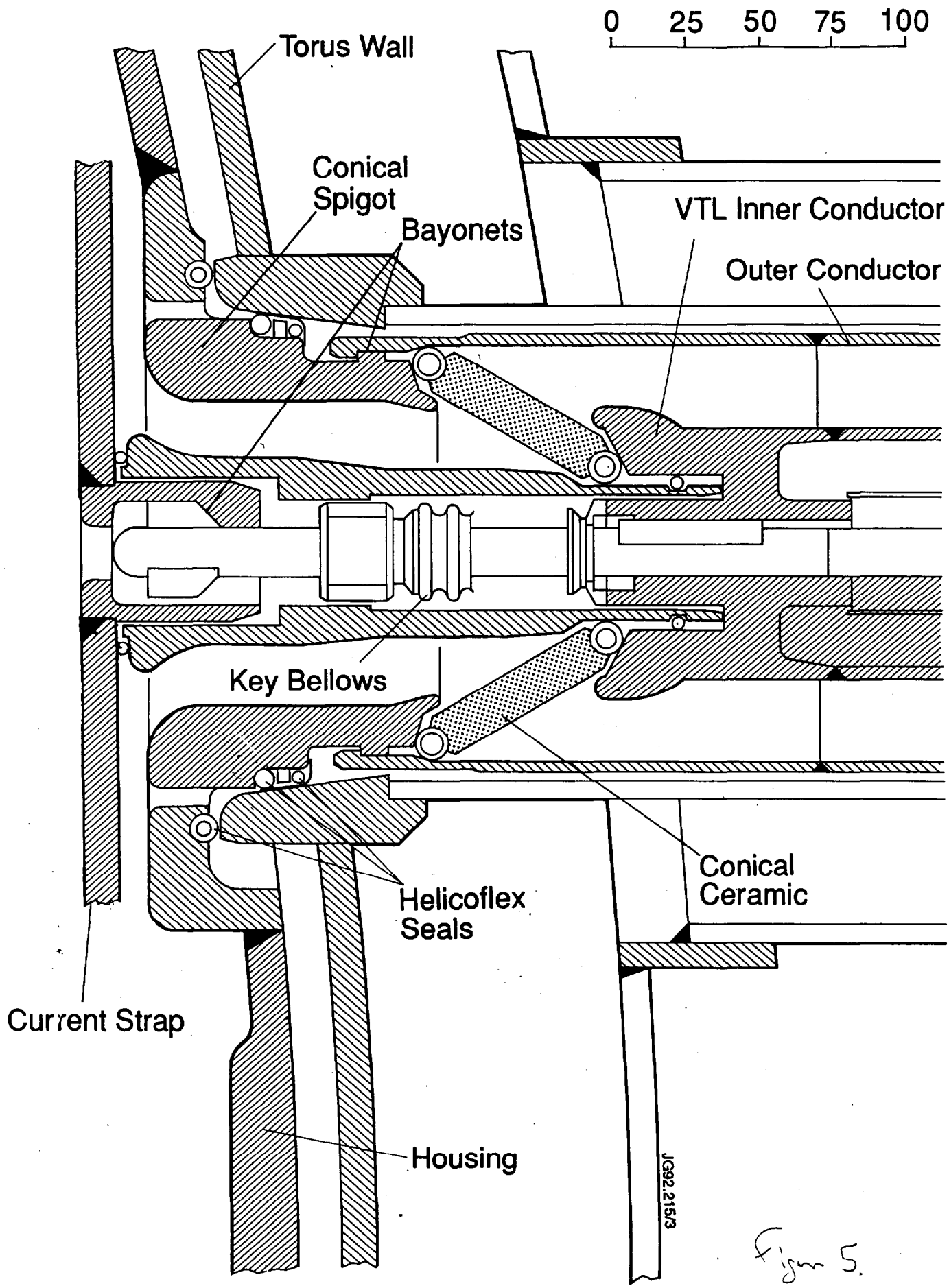
0 25 50 75 100
Torus Wall
Conical
Spigot
Bayonets
VTL Inner Conductor
Outer Conductor
Key Bellows
Conical
Ceramic
Helicoflex
Seals
Current Strap
Housing
JG92.215/3

Figure 5.

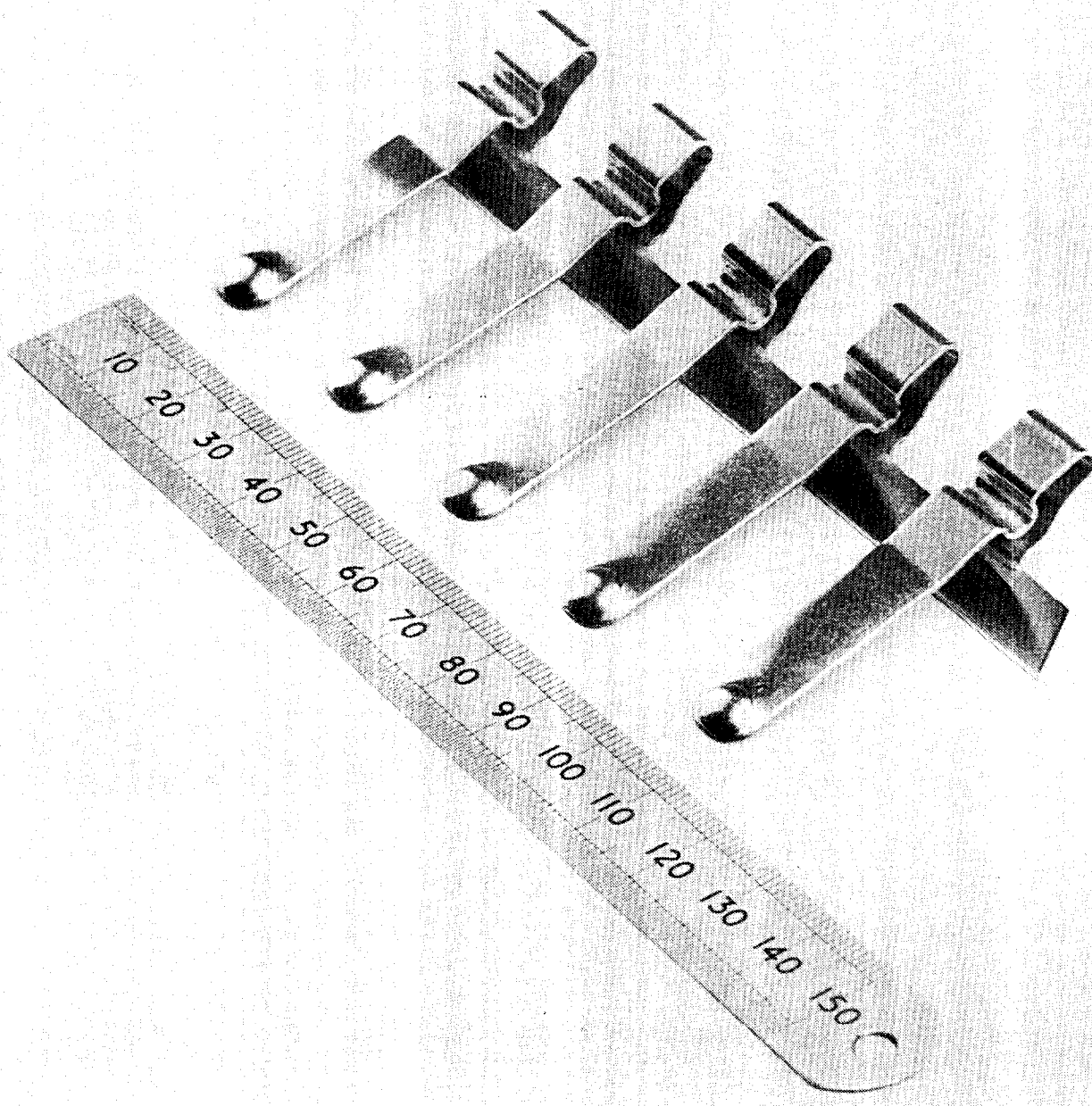

(a)

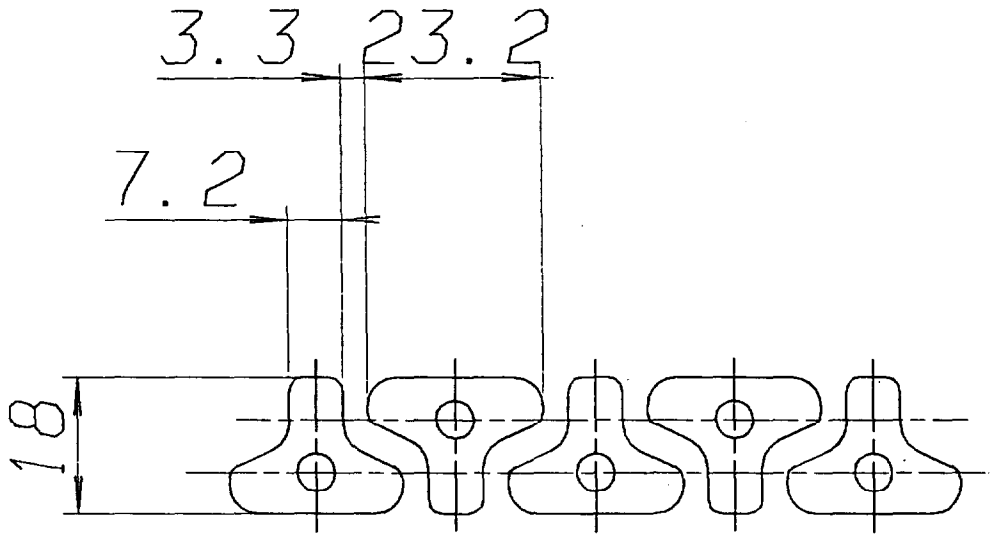

A1, Ni. SCREEN ELEMENT

(b)

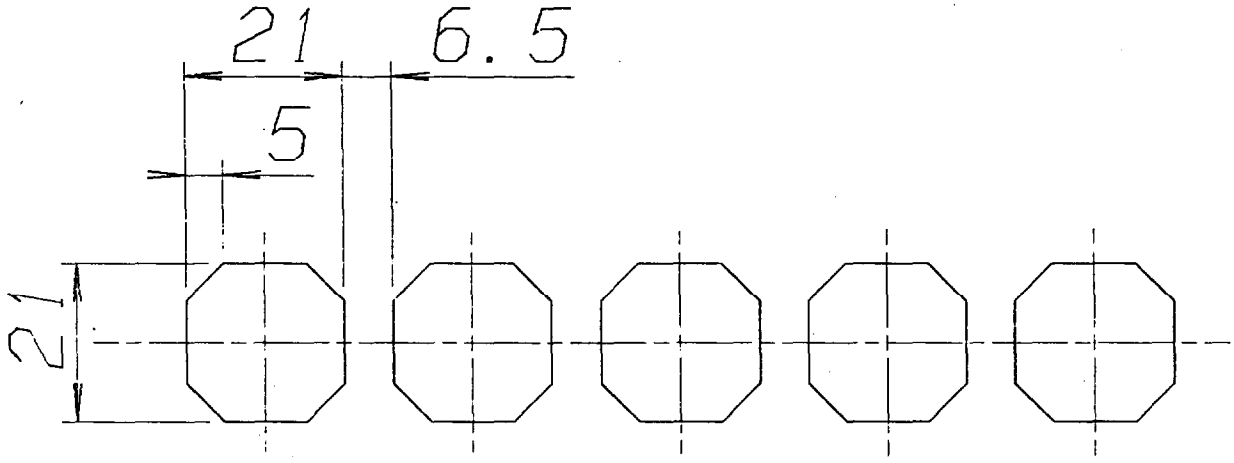

A1, Be. SCREEN ELEMENT

(C)

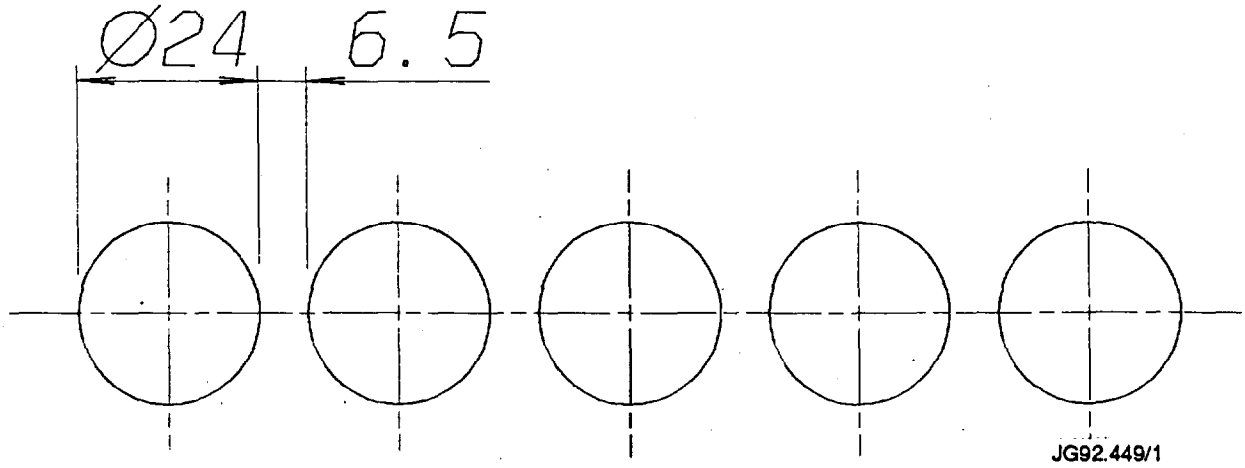

A2, Be. SCREEN ELEMENT

Fig- 7

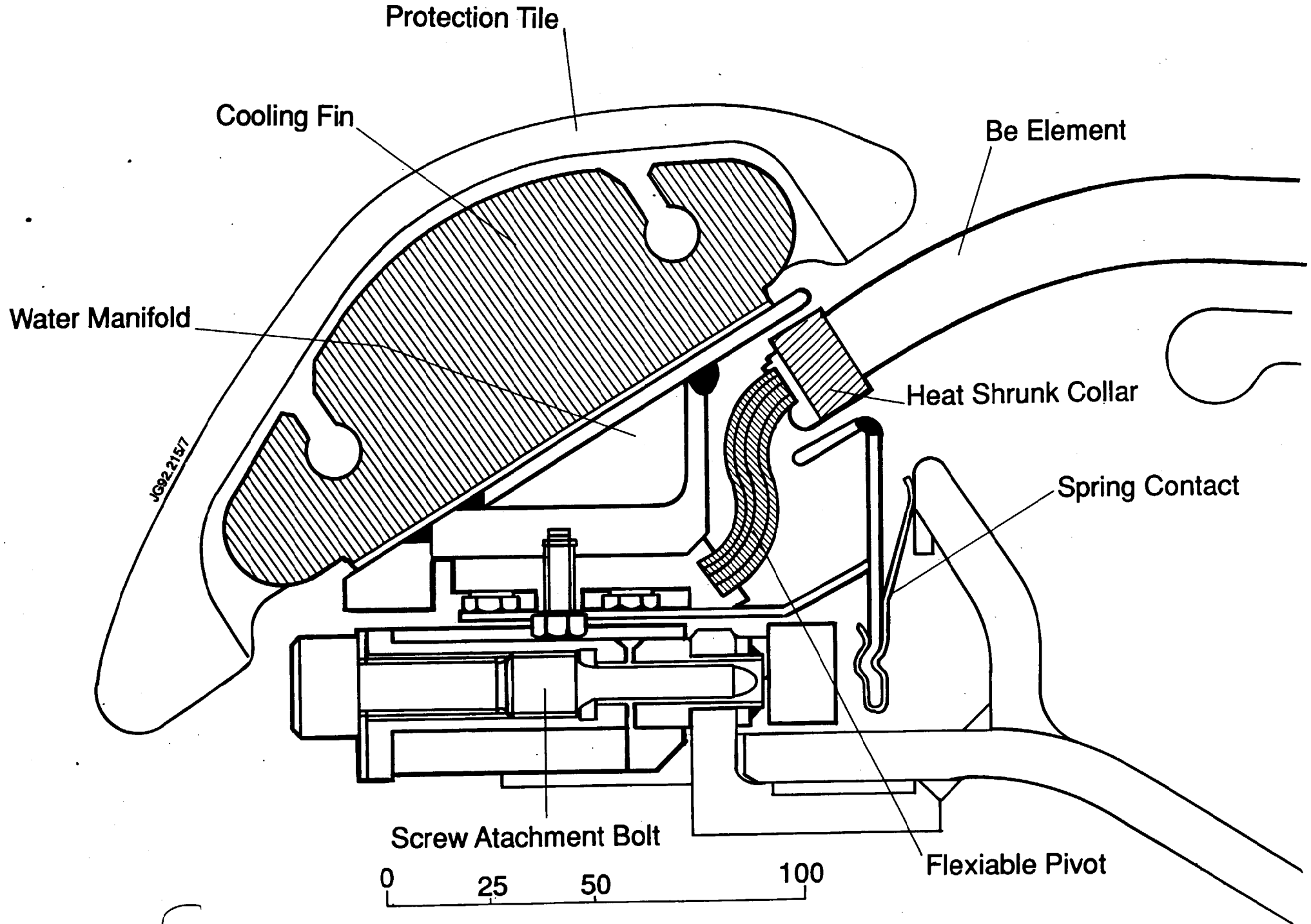
Protection Tile
Cooling Fin
Be Element
Water Manifold
Heat Shrunk Collar
JG92.215/7
Spring Contact
Screw Atachment Bolt
Flexiable Pivot
0
25
50
100

Fig 8.

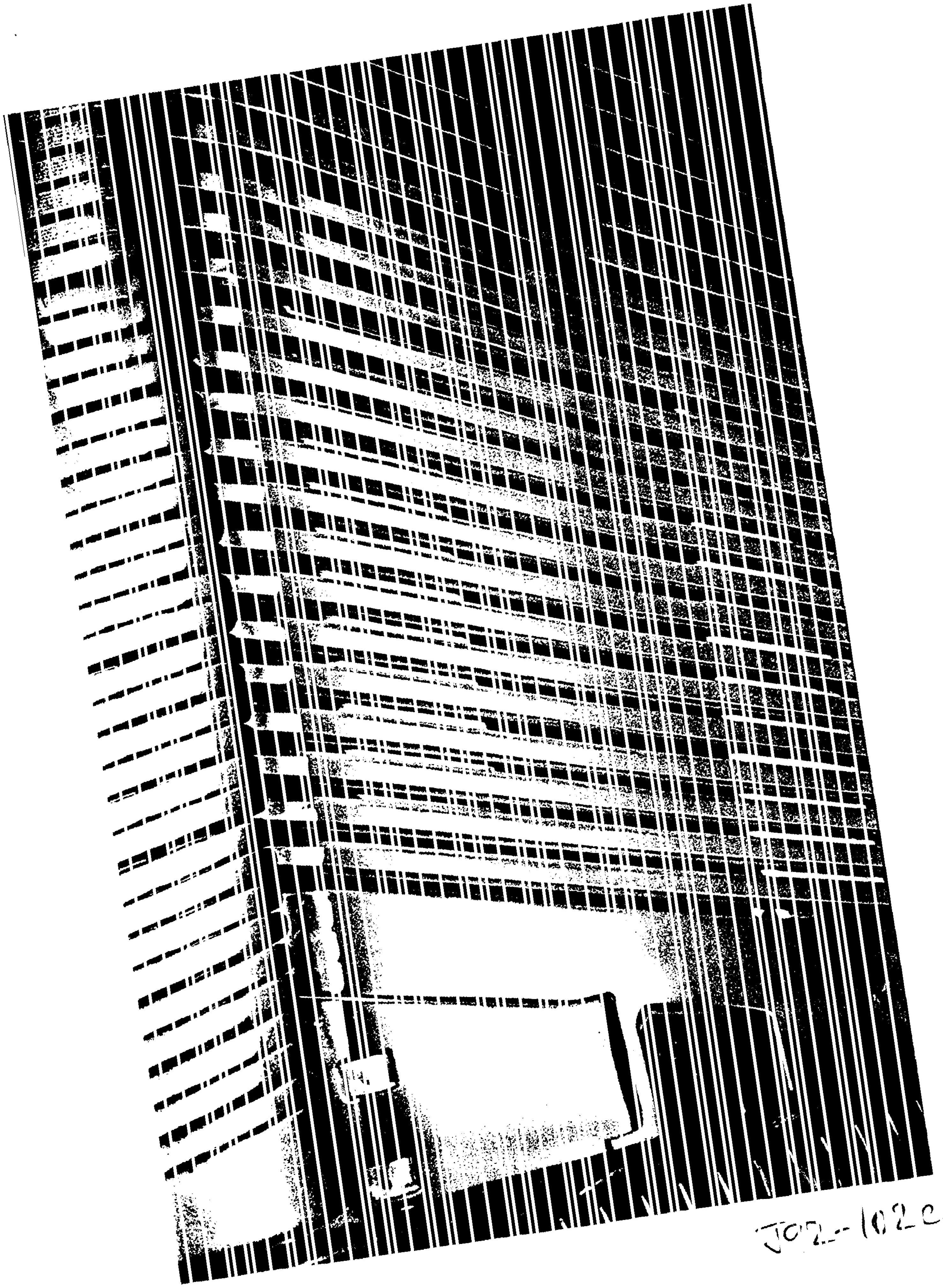

JO2-1020/21A

Fig- 9.

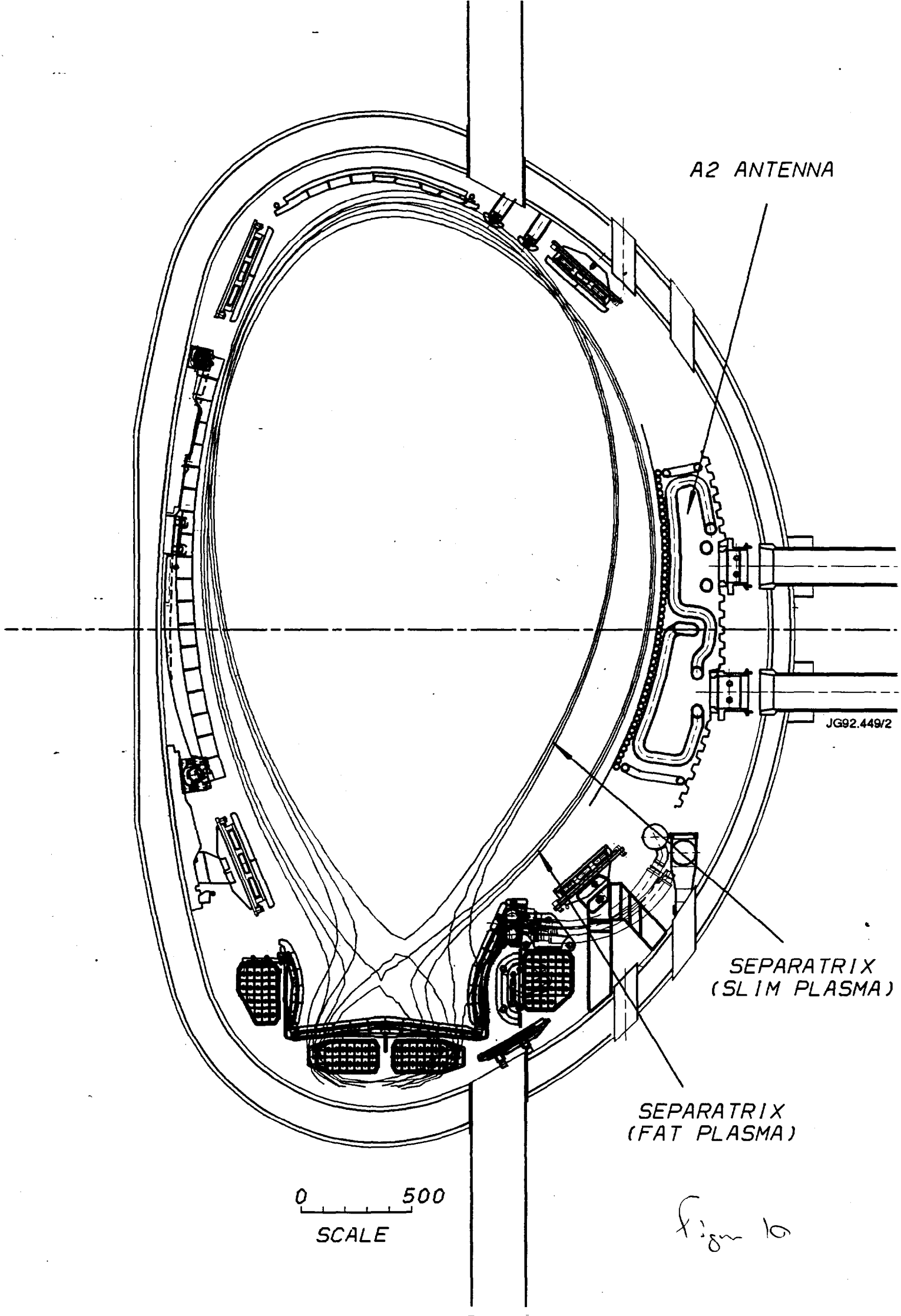
A2 ANTENNA
JG92.449/2
SEPARATRIX
(SLIM PLASMA)
SEPARATRIX
(FAT PLASMA)
0
500
SCALE

Fig 10

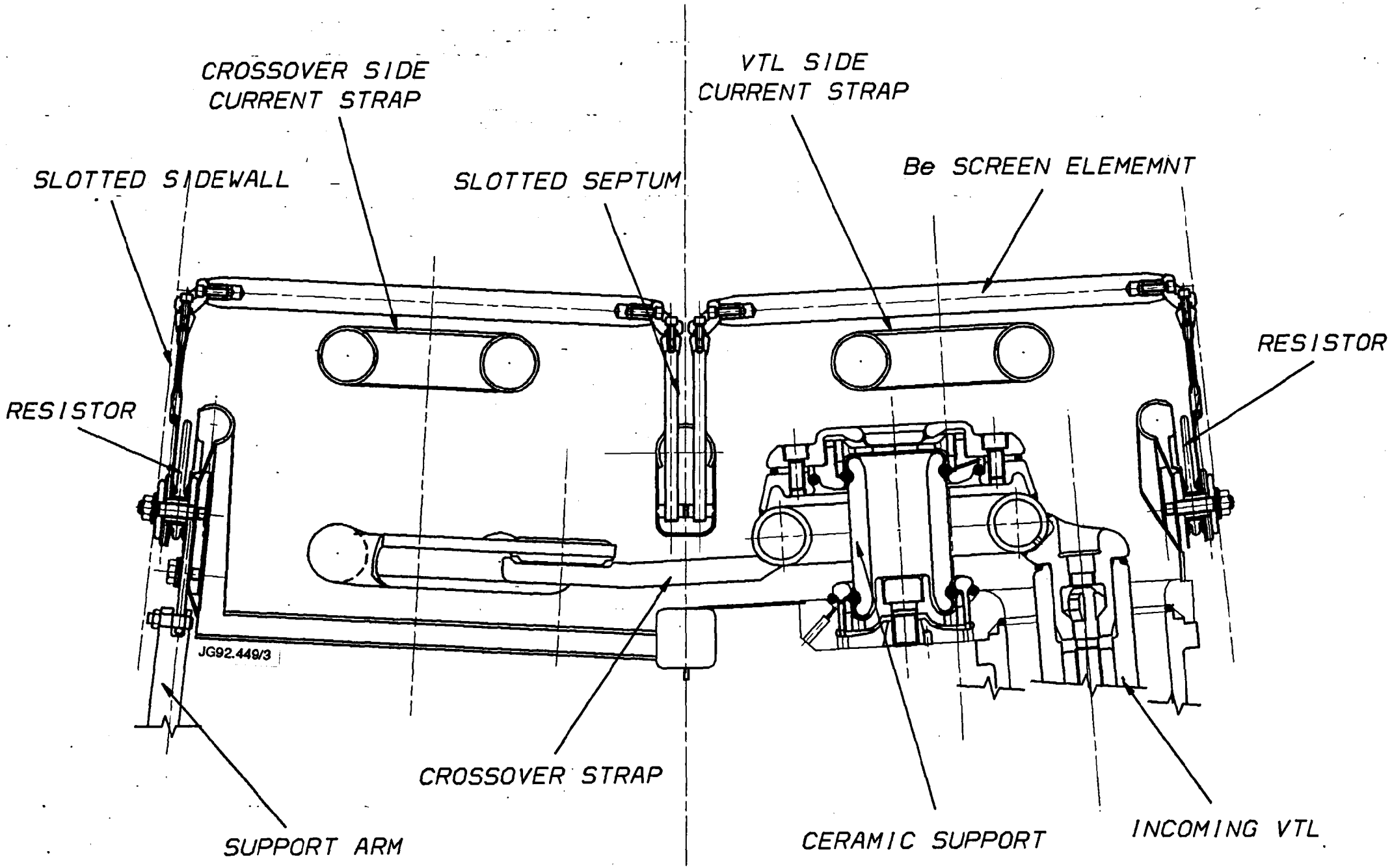
CROSSOVER SIDE
CURRENT STRAP
VTL SIDE
CURRENT STRAP
SLOTTED SIDEWALL
SLOTTED SEPTUM
Be SCREEN ELEMEMNT
RESISTOR
RESISTOR
JG92.449/3
CROSSOVER STRAP
SUPPORT ARM
CERAMIC SUPPORT
INCOMING VTL

Figure 11.

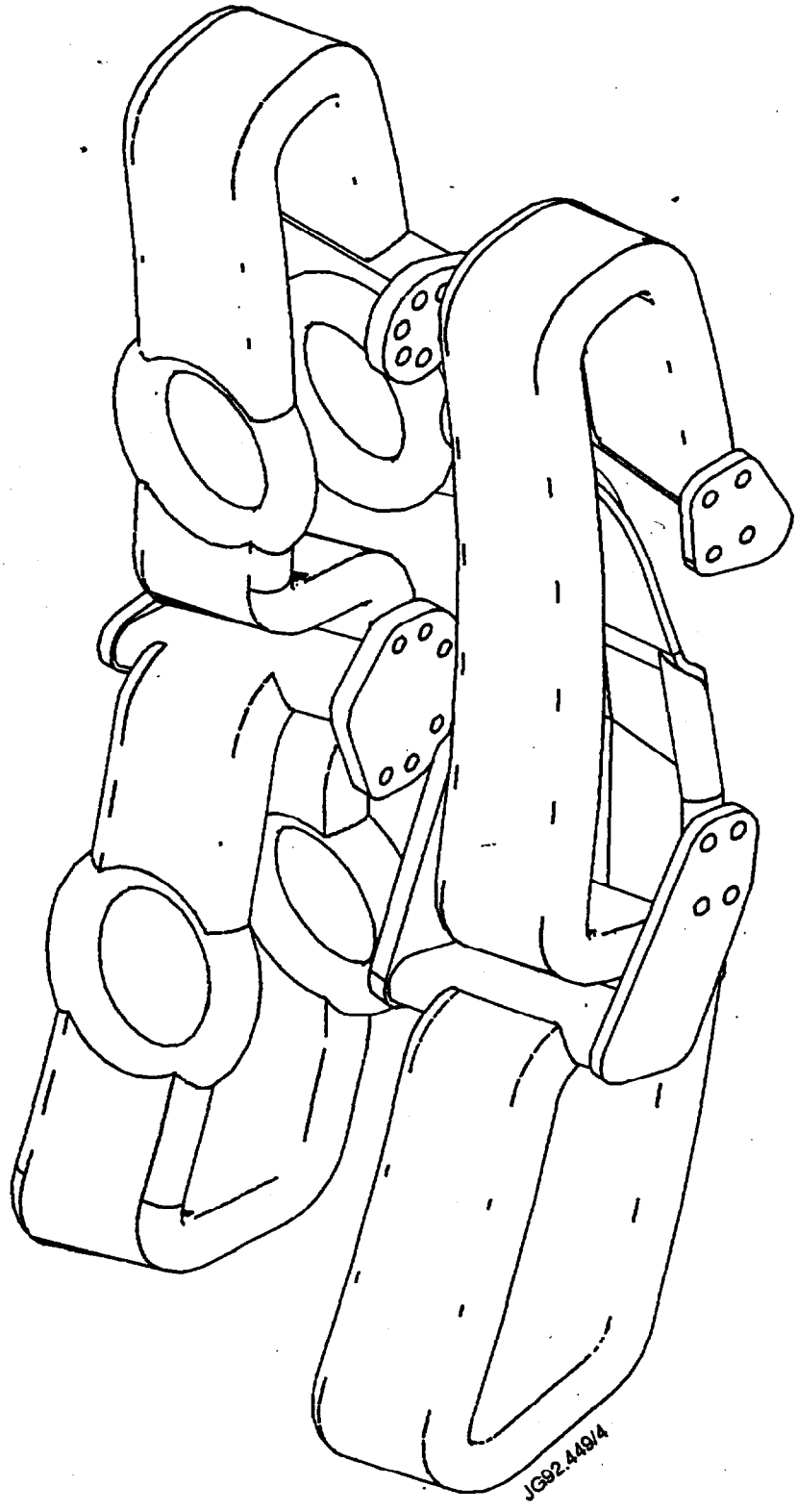

fig 12

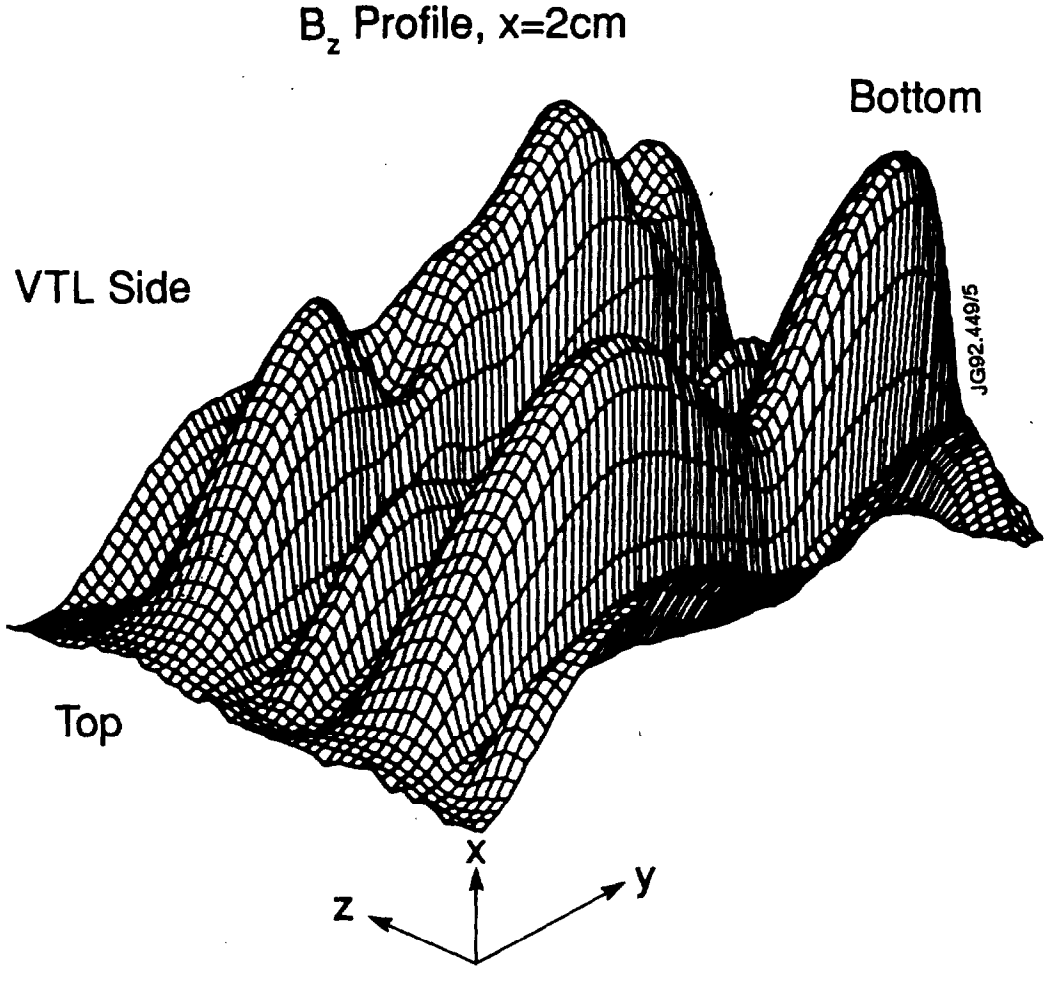

Fig 13.

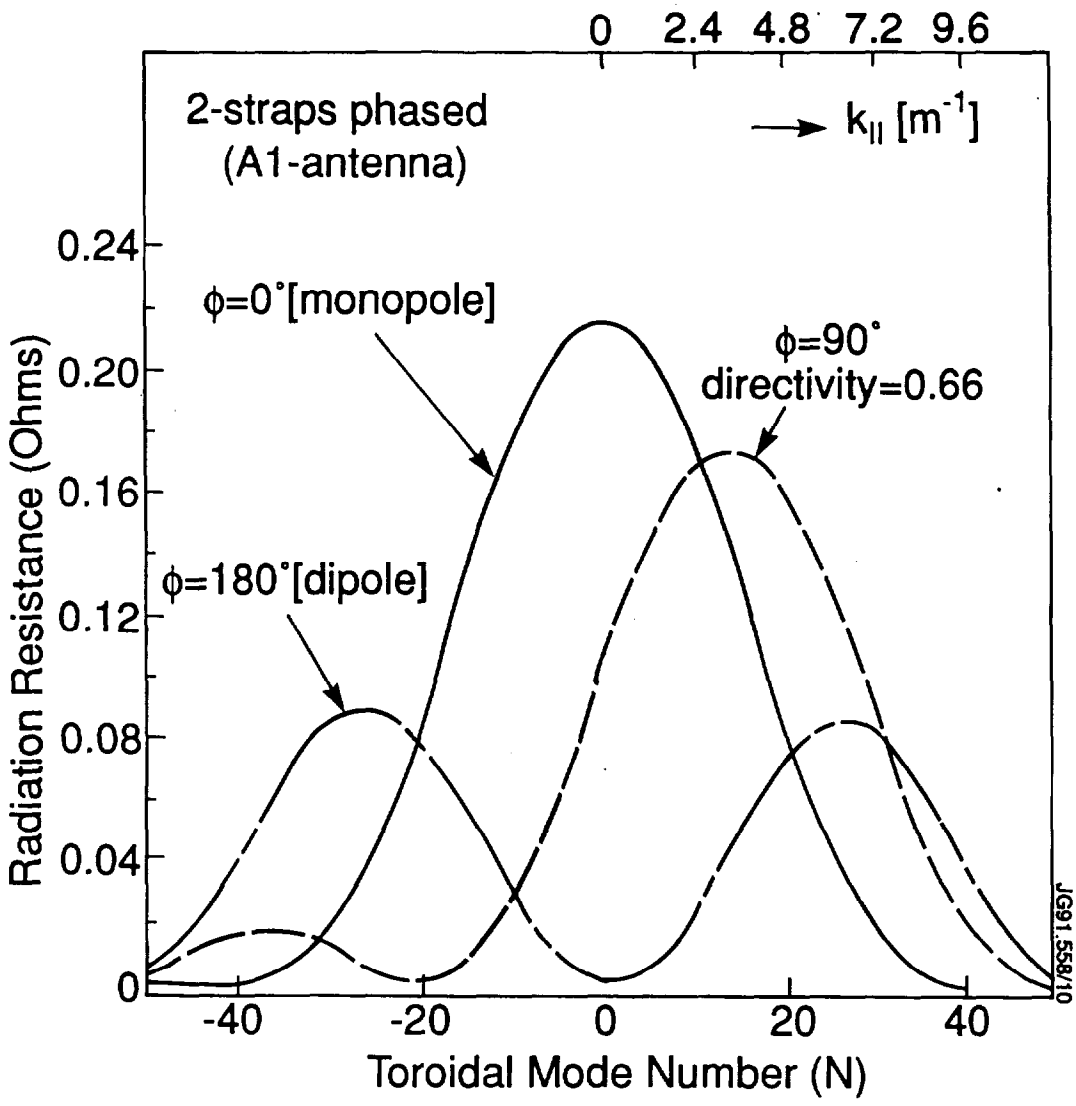
0 2.4 4.8 7.2 9.6
2-straps phased
(A1-antenna)
$k_{||}$ [m^{-1}]
0.24
0.20
0.16
0.12
0.08
0.04
0
Radiation Resistance (Ohms)
ϕ=0°[monopole]
ϕ=90°
directivity=0.66
ϕ=180°[dipole]
-40
-20
0
20
40
Toroidal Mode Number (N)
JG91.558/10

fig 14 a.

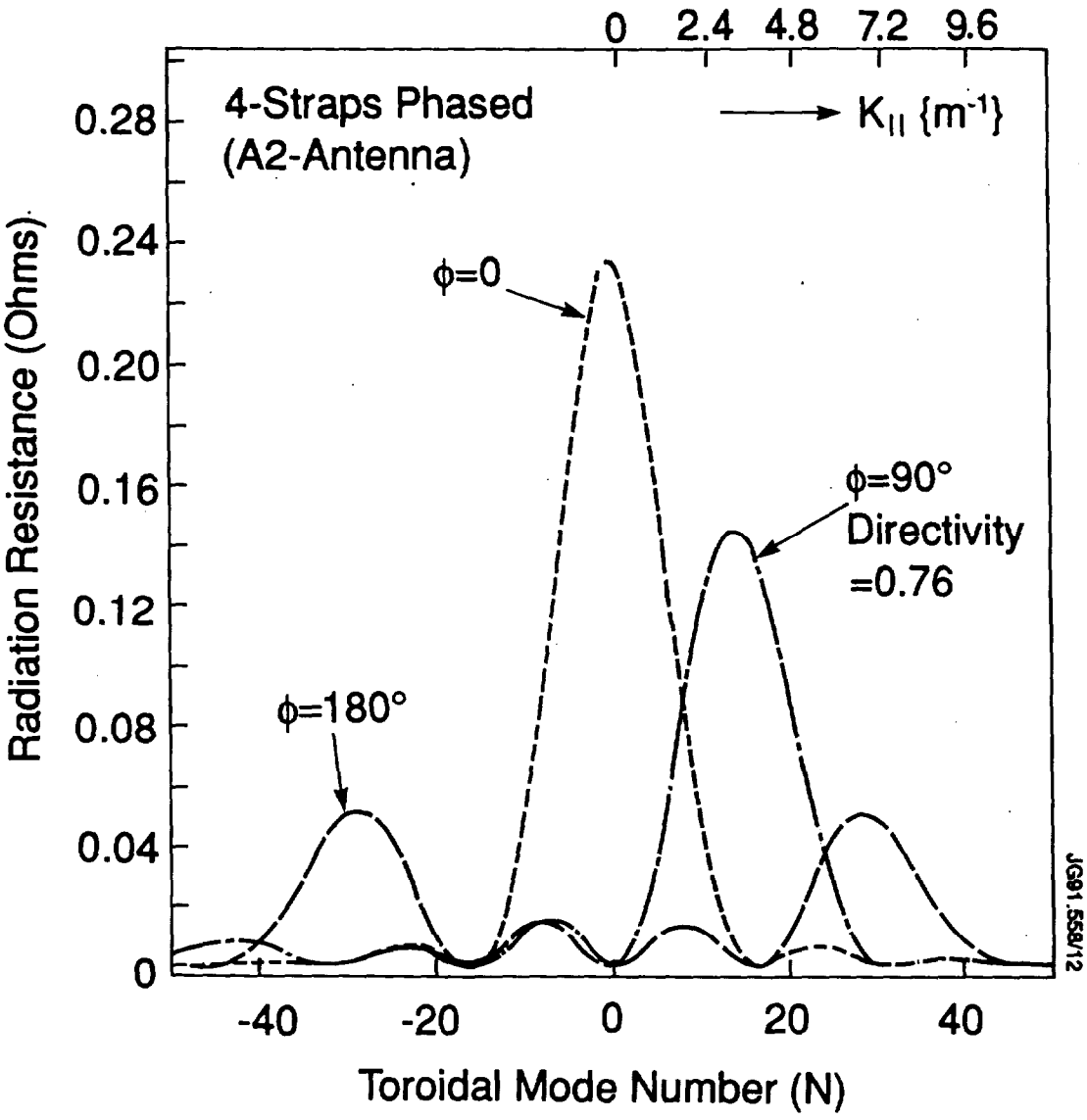
0 2.4 4.8 7.2 9.6
4-Straps Phased
(A2-Antenna)
$K_{||}$ {m^{-1}}
0.28
0.24
0.20
0.16
0.12
0.08
0.04
0
Radiation Resistance (Ohms)
ϕ=0
ϕ=90°
Directivity
=0.76
ϕ=180°
-40 -20 0 20 40
Toroidal Mode Number (N)
JG91.558/12

Fig 14b.

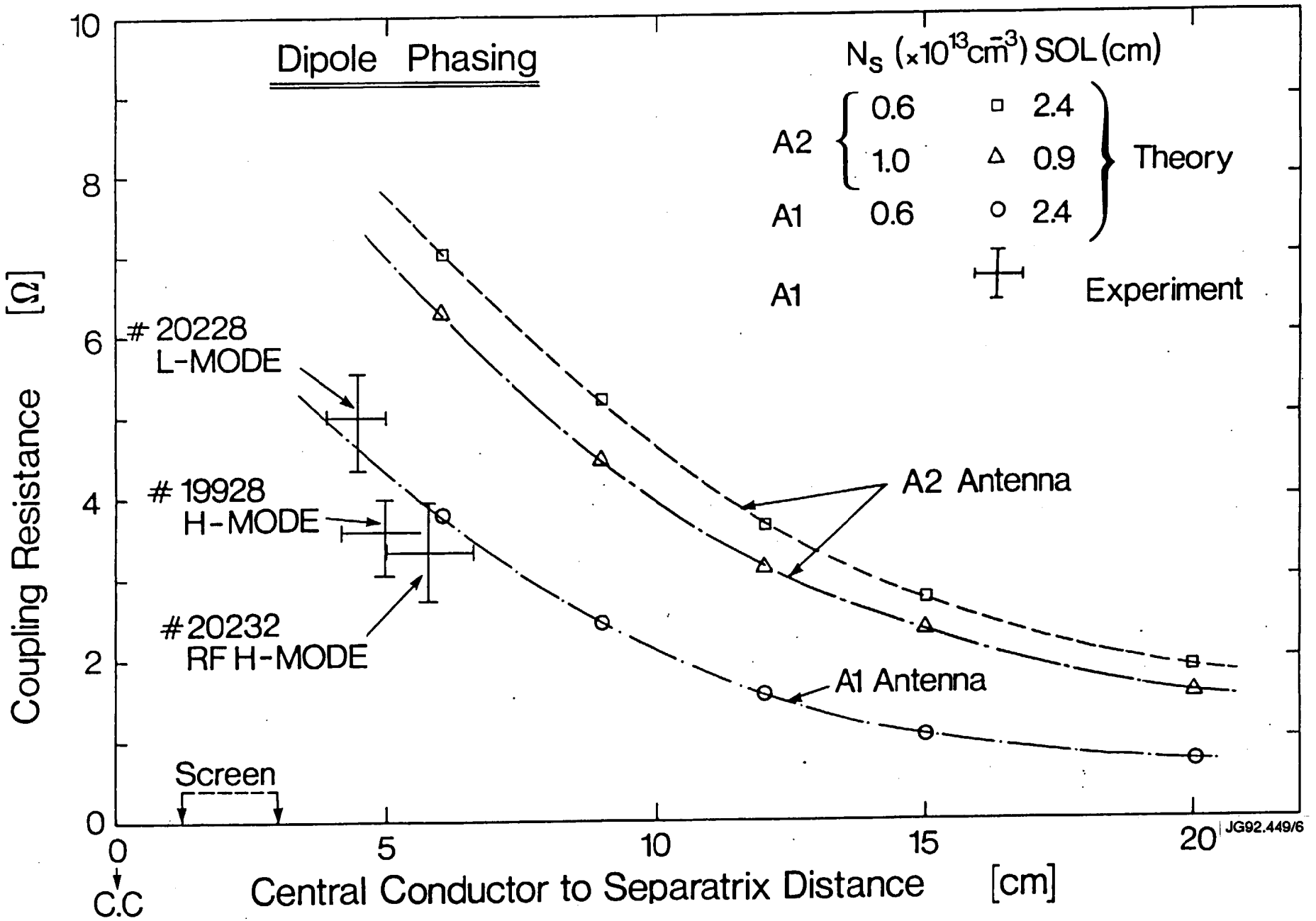
Dipole Phasing
N_s ($\times 10^{13}$cm^{-3}) SOL(cm)
A2
0.6
2.4
1.0
0.9
Theory
A1
0.6
2.4
A1
Experiment
20228
L-MODE
19928
H-MODE
#20232
RF H-MODE
A2 Antenna
A1 Antenna
Screen
Coupling Resistance [Ω]
Central Conductor to Separatrix Distance [cm]
C.C
0
2
4
6
8
10
0
5
10
15
20
JG92.449/6

Fig 15.

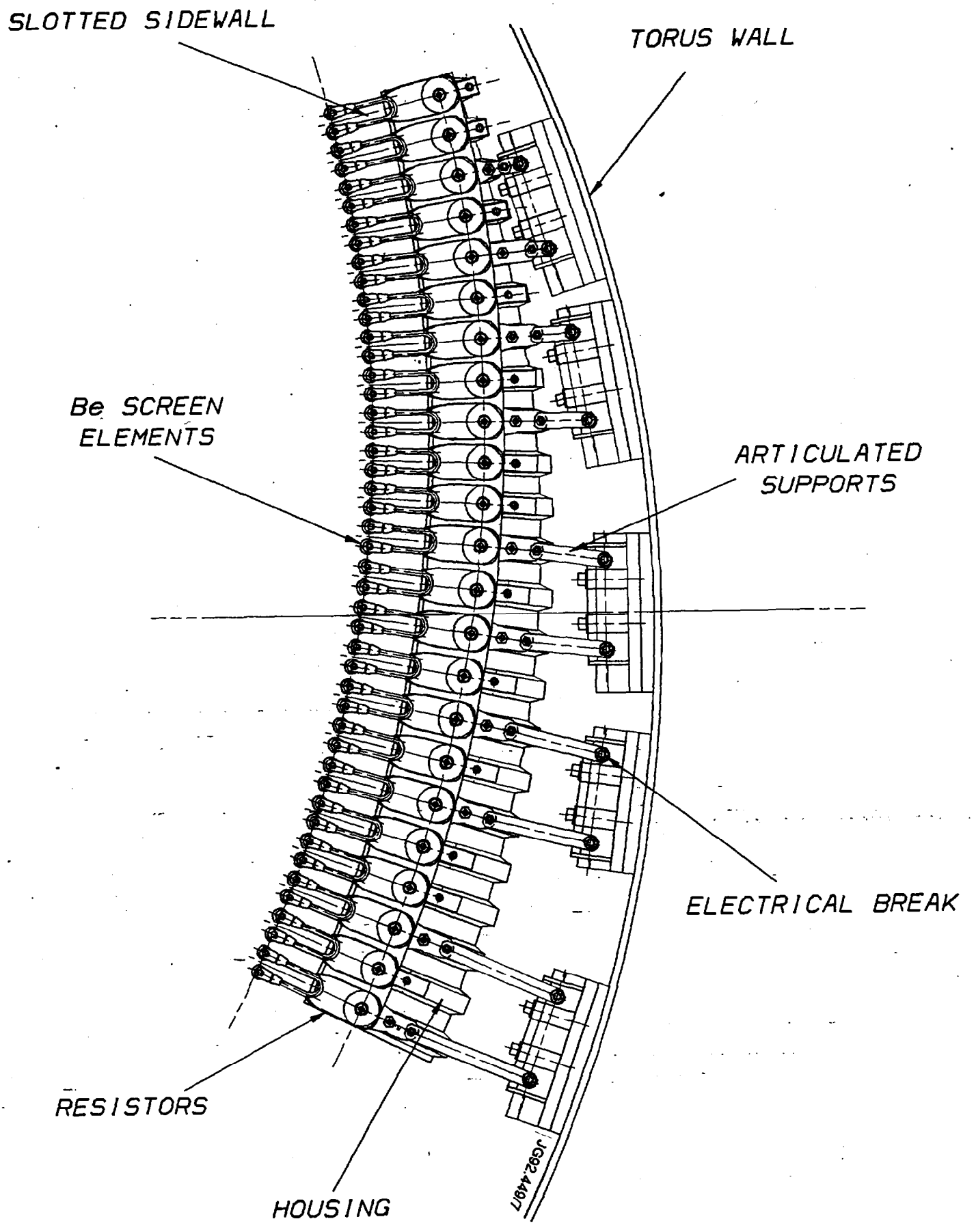
SLOTTED SIDEWALL
TORUS WALL
Be SCREEN ELEMENTS
ARTICULATED SUPPORTS
ELECTRICAL BREAK
RESISTORS
HOUSING
JG92.449/7

Figure 16.

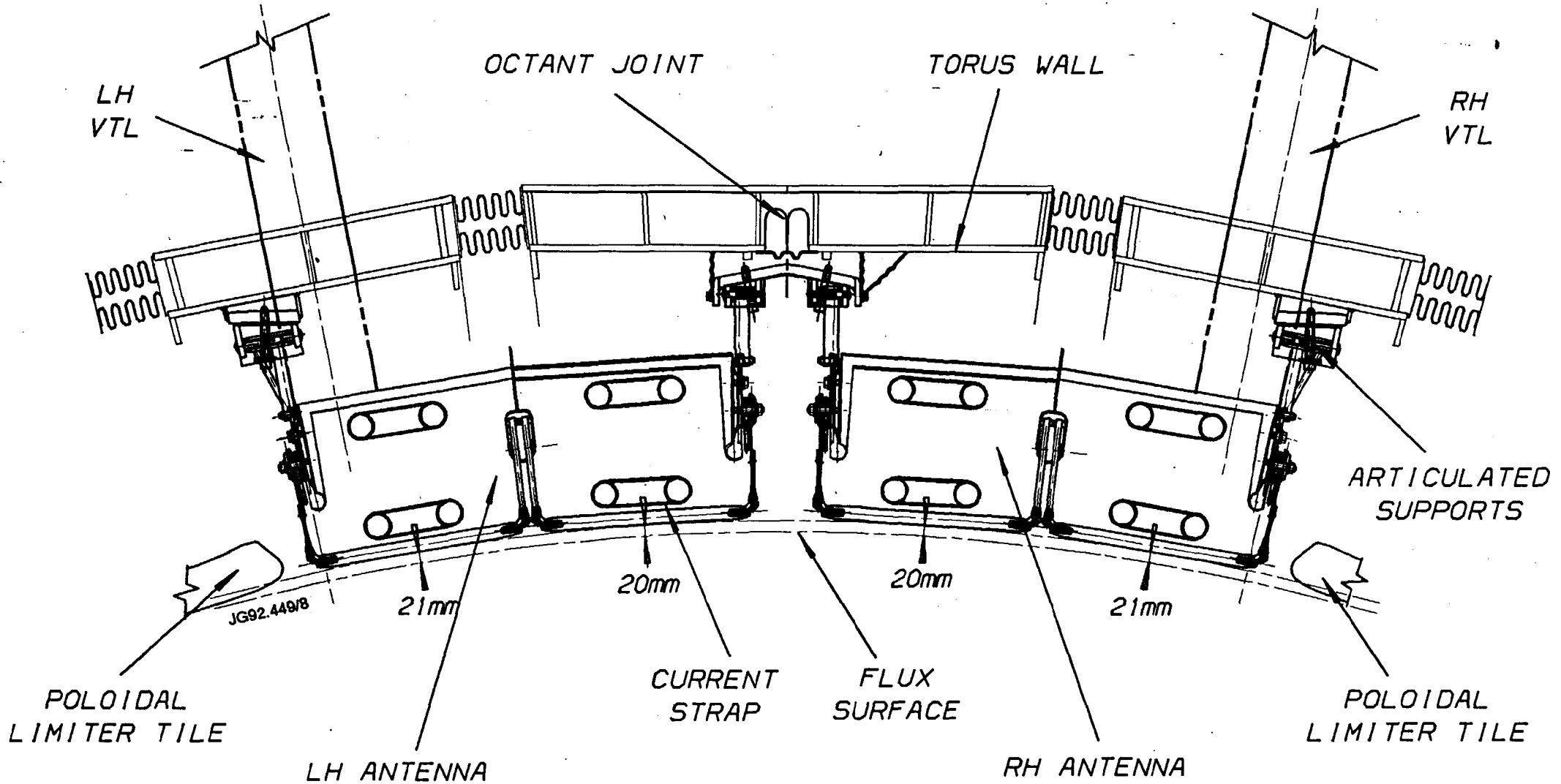
LH
VTL
OCTANT JOINT
TORUS WALL
RH
VTL
ARTICULATED
SUPPORTS
JG92.449/8
21mm
20mm
20mm
21mm
POLOIDAL
LIMITER TILE
LH ANTENNA
CURRENT
STRAP
FLUX
SURFACE
RH ANTENNA
POLOIDAL
LIMITER TILE

f.8. 17

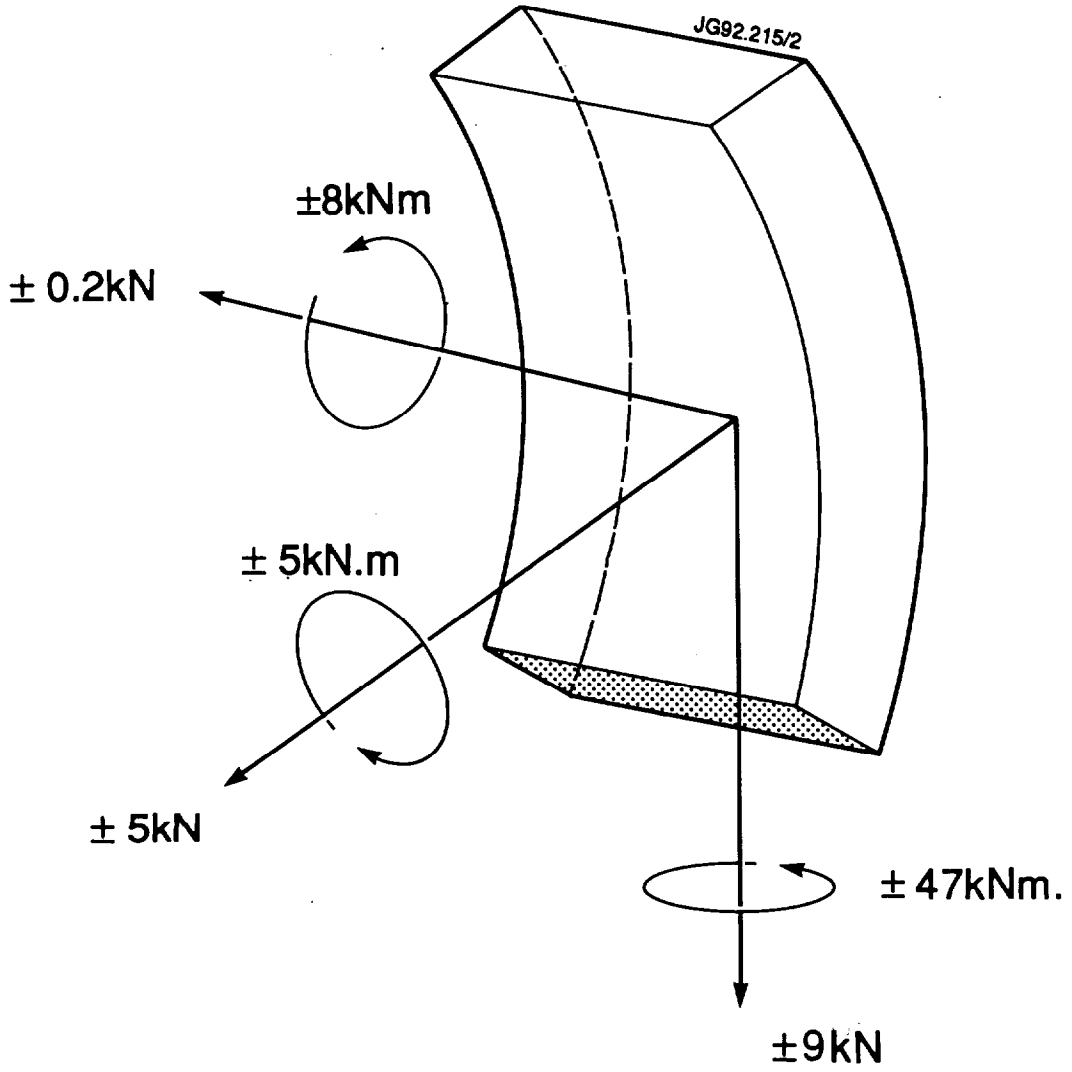

$\dot{B}_v$=120 Tesla / Sec

$\dot{B}_r$=150 Tesla / Sec

Fig 18.

ANNEX

P.-H. REBUT, A. GIBSON, M. HUGUET, J.M. ADAMS[1], B. ALPER, H. ALTMANN, A. ANDERSEN[2], P. ANDREW[3], M. ANGELONE[4], S. ALI-ARSHAD, P. BAIGGER, W. BAILEY, B. BALET, P. BARABASCHI, P. BARKER, R. BARNSLEY[5], M. BARONIAN, D.V. BARTLETT, L. BAYLOR[6], A.C. BELL, G. BENALI, P. BERTOLDI, E. BERTOLINI, V. BHATNAGAR, A.J. BICKLEY, D. BINDER, H. BINDSLEV[2], T. BONICELLI, S.J. BOOTH, G. BOSIA, M. BOTMAN, D. BOUCHER, P. BOUCQUEY, P. BREGER, H. BRELEN, H. BRINKSCHULTE, D. BROOKS, A. BROWN, T. BROWN, M. BRUSATI, S. BRYAN, J. BRZOZOWSKI[7], R. BUCHSE[22], T. BUDD, M. BURES, T. BUSINARO, P. BUTCHER, H. BUTTGEREIT, C. CALDWELL-NICHOLS, D.J. CAMPBELL, P. CARD, G. CELENTANO, C.D. CHALLIS, A.V. CHANKIN[8], A. CHERUBINI, D. CHIRON, J. CHRISTIANSEN, P. CHUILON, R. CLAESEN, S. CLEMENT, E. CLIPSHAM, J.P. COAD, I.H. COFFEY[9], A. COLTON, M. COMISKEY[10], S. CONROY, M. COOKE, D. COOPER, S. COOPER, J.G. CORDEY, W. CORE, G. CORRIGAN, S. CORTI, A.E. COSTLEY, G. COTTRELL, M. COX[11], P. CRIPWELL[12], O. Da COSTA, J. DAVIES, N. DAVIES, H. de BLANK, H. de ESCH, L. de KOCK, E. DEKSNIS, F. DELVART, G.B. DENNE-HINNOV, G. DESCHAMPS, W.J. DICKSON[13], K.J. DIETZ, S.L. DMITRENKO, M. DMITRIEVA[14], J. DOBBING, A. DOGLIO, N. DOLGETTA, S.E. DORLING. P.G. DOYLE, D.F. DÜCHS, H. DUQUENOY, A. EDWARDS, J. EHRENBERG, A. EKEDAHL, T. ELEVANT[7], S.K. ERENTS[11], L.G. ERIKSSON, H. FAJEMIROKUN[12], H. FALTER, J. FREILING[15], F. FREVILLE, C. FROGER, P. FROISSARD, K. FULLARD, M. GADEBERG, A. GALETSAS, T. GALLAGHER, D. GAMBIER, M. GARRIBBA, P. GAZE, R. GIANNELLA, R.D. GILL, A GIRARD, A. GONDHALEKAR, D. GOODALL[11], C. GORMEZANO, N.A. GOTTARDI, C. GOWERS, B.J. GREEN, B. GRIEVSON, R. HAANGE, A. HAIGH, C.J. HANCOCK, P.J. HARBOUR, T. HARTRAMPF, N.C. HAWKES[11], P. HAYNES[11], J.L. HEMMERICH, T. HENDER[11], J. HOEKZEMA, D. HOLLAND, M. HONE, L. HORTON, J. HOW, M. HUART, I. HUGHES, T.P. HUGHES[10], M. HUGON, Y. HUO[16], K. IDA[17], B. INGRAM, M. IRVING, J. JACQUINOT, H. JAECKEL, J.F. JAEGER, G. JANESCHITZ, Z. JANKOVICZ[18], O.N. JARVIS, F. JENSEN, E.M. JONES, H.D. JONES, L.P.D.F. JONES, S. JONES[19], T.T.C. JONES, J.-F. JUNGER, F. JUNIQUE, A. KAYE, B.E. KEEN, M. KEILHACKER, G.J. KELLY, W. KERNER, A. KHUDOLEEV[21], R. KONIG, A. KONSTANTELLOS, M. KOVANEN[20], G. KRAMER[15], P. KUPSCHUS, R. LÄSSER, J.R. LAST, B. LAUNDY, L. LAURO-TARONI, M. LAVEYRY, K. LAWSON[11], M. LENNHOLM, J. LINGERTAT[22], R.N. LITUNOVSKI, A. LOARTE, R. LOBEL, P. LOMAS, M. LOUGHLIN, C. LOWRY, J. LUPO, A.C. MAAS[15], J. MACHUZAK[19], B. MACKLIN, G. MADDISON[11], C.F. MAGGI[23], G. MAGYAR, W. MANDL[22], V. MARCHESE, G. MARCON, F. MARCUS, J. MART, D. MARTIN, E. MARTIN, R. MARTIN-SOLIS[24], P. MASSMANN, G. MATTHEWS, H. McBRYAN, G. McCRACKEN[11], J. McKIVITT, P. MERIGUET, P. MIELE, A. MILLER, J. MILLS, S.F. MILLS, P. MILLWARD, P. MILVERTON, E. MINARDI[4], R. MOHANTI[25], P.L. MONDINO, D. MONTGOMERY[26], A. MONTVAI[27], P. MORGAN, H. MORSI, D. MUIR, G. MURPHY, R. MYRNÄS[28], F. NAVE[29], G. NEWBERT, M. NEWMAN, P. NIELSEN, P. NOLL, W. OBERT, D. O'BRIEN, J. ORCHARD, J. O'ROURKE, R. OSTROM, M. OTTAVIANI, M. PAIN, F. PAOLETTI, S. PAPASTERGIOU, W. PARSONS, D. PASINI, D. PATEL, A. PEACOCK, N. PEACOCK[11], R.J.M. PEARCE, D. PEARSON[12], J.F. PENG[16], R. PEPE DE SILVA, G. PERINIC, C. PERRY, M. PETROV[21], M.A. PICK, J. PLANCOULAINE, J.-P POFFÉ, R. PÖHLCHEN, F. PORCELLI, L. PORTE[13], R. PRENTICE, S. PUPPIN, S. PUTVINSKII[8], G. RADFORD[30], T. RAIMONDI, M.C. RAMOS DE ANDRADE, R. REICHLE, J. REID, S. RICHARDS, E. RIGHI, F. RIMINI, D. ROBINSON[11], A. ROLFE, R.T. ROSS, L. ROSSI, R. RUSS, P. RUTTER, H.C. SACK, G. SADLER, G. SAIBENE, J.L. SALANAVE, G. SANAZZARO, A. SANTAGIUSTINA, R. SARTORI, C. SBORCHIA, P. SCHILD, M. SCHMID, G. SCHMIDT[31], B. SCHUNKE, S.M. SCOTT, L. SERIO, A SIBLEY, R. SIMONINI, A.C.C. SIPS, P. SMEULDERS, R. SMITH, R. STAGG, M. STAMP, P. STANGEBY[3], R. STANKIEWICZ[32], D.F. START, C.A. STEED, D. STORK, P.E. STOTT, P. STUBBERFIELD, D. SUMMERS, H. SUMMERS[13], L. SVENSSON, J.A. TAGLE[33], M. TALBOT, A. TANGA, A. TARONI, C. TERELLA, A TERRINGTON, A TESINI, P.R. THOMAS, E. THOMPSON, K. THOMSEN, F. TIBONE, A. TISCORNIA, P. TREVALION, B. TUBBING, P. VAN BELLE, H. VAN DER BEKEN, G. VLASES, M. VON HELLERMANN, T. WADE, C. WALKER, R. WALTON[31], D. WARD, M.L. WATKINS, N. WATKINS, M.J. WATSON, S. WEBER[34], J. WESSON, T.J. WIJNANDS, J. WILKS, D. WILSON, T. WINKEL, R. WOLF, D. WONG, C. WOODWARD, Y. WU[35], M. WYKES, D. YOUNG, I.D. YOUNG, L. ZANNELLI, A. ZOLFAGHARI[19], W. ZWINGMANN

[1] Harwell Laboratory, UKAEA, Harwell, Didcot, Oxfordshire, UK.
[2] Risø National Laboratory, Roskilde, Denmark.
[3] Institute for Aerospace Studies, University of Toronto, Downsview, Ontario, Canada.
[4] ENEA Frascati Energy Research Centre, Frascati, Rome, Italy.
[5] University of Leicester, Leicester, UK.
[6] Oak Ridge National Laboratory, Oak Ridge, TN, USA.
[7] Royal Institute of Technology, Stockholm, Sweden.
[8] I.V. Kurchatov Institute of Atomic Energy, Moscow, Russian Federation.
[9] Queens University, Belfast, UK.
[10] University of Essex, Colchester, UK.
[11] Culham Laboratory, UKAEA, Abingdon, Oxfordshire, UK.
[12] Imperial College of Science, Technology and Medicine, University of London, London, UK.
[13] University of Strathclyde, Glasgow, UK.
[14] Keldysh Institute of Applied Mathematics, Moscow, Russian Federation.
[15] FOM-Institute for Plasma Physics "Rijnhuizen", Nieuwegein, Netherlands.
[16] Institute of Plasma Physics, Academia Sinica, Hefei, Anhui Province, China.
[17] National Institute for Fusion Science, Nagoya, Japan.
[18] Soltan Institute for Nuclear Studies, Otwock/Świerk, Poland.
[19] Plasma Fusion Center, Massachusetts Institute of Technology, Boston, MA, USA.
[20] Nuclear Engineering Laboratory, Lappeenranta University, Finland.
[21] A.F. Ioffe Physico-Technical Institute, St. Petersburg, Russian Federation.
[22] Max-Planck-Institut für Plasmaphysik, Garching, Germany.
[23] Department of Physics, University of Milan, Milan, Italy.
[24] Universidad Complutense de Madrid, Madrid, Spain.
[25] North Carolina State University, Raleigh, NC, USA.
[26] Dartmouth College, Hanover, NH, USA.
[27] Central Research Institute for Physics, Budapest, Hungary.
[28] University of Lund, Lund, Sweden.
[29] Laboratorio Nacional de Engenharia e Tecnologia Industrial, Sacavem, Portugal.
[30] Institute of Mathematics, University of Oxford, Oxford, UK.
[31] Princeton Plasma Physics Laboratory, Princeton University, Princeton, NJ, USA.
[32] RCC Cyfronet, Otwock/Świerk, Poland,
[33] Centro de Investigaciones Energéticas, Medioambientales y Tecnológicas, Madrid, Spain.
[34] Freie Universität, Berlin, Germany.
[35] Insitute for Mechanics, Academia Sinica, Beijing, China.